

Multi-wavelength Probes of Obscuration Towards the Narrow Line Region in Seyfert Galaxies

S. B. Kraemer¹, H.R. Schmitt², D. M. Crenshaw³, M. Meléndez⁴, T.J. Turner⁵, M. Guainazzi⁶, & R.F. Mushotzky⁷

ABSTRACT

We present a study of reddening and absorption towards the Narrow Line Regions (NLR) in active galactic nuclei (AGN) selected from the Revised Shapley-Ames, 12 μ m, and *Swift*/Burst Alert Telescope samples. For the sources in host galaxies with inclinations of $b/a > 0.5$, we find that mean ratio of [O III] λ 5007, from ground-based observations, and [O IV] 28.59 μ m, from *Spitzer*/Infrared Spectrograph observations, is a factor of 2 lower in Seyfert 2s than Seyfert 1s. The combination of low [O III]/[O IV] and [O III] λ 4363/ λ 5007 ratios in Seyfert 2s suggests more extinction of emission from the NLR than in Seyfert 1s. Similar column densities of dusty gas, $N_H \sim \text{several} \times 10^{21} \text{ cm}^{-2}$, can account for the suppression of both [O III] λ 5007 and [O III] λ 4363, as compared to those observed in Seyfert 1s. Also, we find that the X-ray line O VII λ 22.1 Å is weaker in Seyfert 2s, consistent with absorption by the same gas that reddens the optical emission. Using a *Hubble Space Telescope*/Space Telescope Imaging Spectrograph slitless spectrum of the Seyfert 1 galaxy NGC 4151, we estimate that only $\sim 30\%$ of the [O III] λ 5007 comes from within 30 pc of the central source, which is insufficient to account for the low [O III]/[O IV] ratios in Seyfert

¹Institute for Astrophysics and Computational Sciences, Department of Physics, The Catholic University of America, Washington, DC 20064; and Code 667, Astrophysics Science Division, NASA Goddard Space Flight Center, Greenbelt, MD 20771.

²Remote Sensing Division, Naval Research Laboratory, Washington, DC 20375; and Computational Physics Inc., Springfield, VA 22151.

³Department of Physics and Astronomy, Georgia State University, Astronomy Offices, Atlanta, GA 30303.

⁴Henry A. Rowland Dept. of Physics & Astronomy, The Johns Hopkins University, Homewood Campus, Baltimore, MD 21218

⁵Dept. of Physics, University of Maryland Baltimore County, Baltimore, MD 21250

⁶European Space Astronomy Centre of the European Space Agency, PO Box 78, Villanueva de la Cañada, e-28691 Madrid, Spain

⁷Department of Astronomy, University of Maryland, College Park, MD 20742

2s. If Seyfert 2 galaxies have similar intrinsic [O III] spatial profiles, the external dusty gas must extend further out along the NLR, perhaps in the form of nuclear dust spirals that have been associated with fueling flows towards the AGN.

1. Introduction

Seyfert galaxies are relatively moderate luminosity ($L_{bol} \lesssim 10^{45}$ ergs $^{-1}$), local ($z < 0.1$) AGN. Historically, they have been classified based on their optical spectra, with Seyfert 1s possessing broad permitted lines (full width at half maximum [FWHM] \gtrsim few 1000 km s $^{-1}$), narrower forbidden lines (FWHM \lesssim 1000 km s $^{-1}$) and non-stellar continua, and Seyfert 2s possessing permitted and forbidden lines of similar widths and optical continua dominated by the host galaxy (Khachikian & Weedman 1974). The discovery of polarized broad permitted lines and non-stellar continua in spectro-polarimetric observations of Seyfert 2 galaxies (e.g., Miller & Antonucci 1983) led to the unified model for Seyfert galaxies (Antonucci 1993), which posits that the central AGN is surrounded by a dusty, molecular torus and the difference between the two types is due to our line of sight with respect to the torus. Specifically, our view of the broad emission line region and central continuum source in Seyfert 2s is blocked by the torus in the above picture.

The forbidden lines detected in Seyfert galaxies arise from the so-called narrow-line region (NLR) which may extend from 1pc to several hundred pcs from the central source. Based on narrow-band [O III] images, originally from ground-based observations (Pogge 1988a,b; 1989) and, subsequently images obtained with the *Hubble Space Telescope (HST)* (Schmitt & Kinney (1996), the NLR in many Seyferts exhibits a bi-conical structure, consistent with collimation of the ionizing radiation emitted by the central source, either by the torus or an optically thick wind emanating from the accretion disk (e.g. Königl & Kartje 1994). Depending on the scale height of the torus, one would expect that the Seyfert 1s and 2s would exhibit similar NLR emission-line properties, while their structure should depend primarily on viewing angle, with Seyfert 1s being more symmetric and compact. While the latter is generally the case (Schmitt et al. 2003a), with some caveats (e.g. Mulchaey et al. 1994), there are clear differences in the emission-line spectra. Nagao et al. (2001) have shown that the density-sensitive [O III] $\lambda 4363/\lambda 5007$ ratio (hereafter, R_{O3}) is greater in Seyfert 1s, indicating the contribution from gas with density $n_H > 10^{5.5}$ cm $^{-3}$, the critical density for de-excitation of the 1D_2 level of O III (Osterbrock & Ferland 2006). Furthermore, high ionization lines such as [Fe X] $\lambda 6374$ are relatively stronger in Seyfert 1s. Nagao et al. speculate that the dense [O III]-emitting region and the high ionization gas are in the inner part of the NLR, and hence may be obscured by the torus in Seyfert 2s. The relationship between

the FWHM of emission lines, detected in the spectra of Seyfert galaxies, and the critical densities of their upper levels (e.g., Filippenko & Halpern 1984; de Robertis & Osterbrock 1986), is further evidence for density stratification in the NLR.

The putative torus, however, may not be the only source of extinction towards the emission-line regions in Seyfert galaxies. There appears to be dust in our line-of-sight towards the NLR of Seyfert galaxies, with reddening of $E_{B-V} \sim 0.2 - 0.4$ mag (e.g., Cohen 1983; MacAlpine 1988; Ferland & Osterbrock 1986; Kraemer et al. 1994). In our analysis (Kraemer & Crenshaw 2000a) of long slit spectra of the NLR of the Seyfert 2 galaxy NGC 1068, obtained with *HST*/Space Telescope Imaging Spectrograph (STIS), we found extinction of the optical and UV emission lines consistent with a “screen” of dust¹, external to the optical NLR, with a hydrogen column density $N_H \sim 10^{21} \text{ cm}^{-2}$, assuming a Galactic dust-to-gas ratio (Shull & van Steenberg 1985). On the other hand, while there is less evidence for an external screen in the Seyfert 1 galaxy NGC 4151 (Kraemer et al. 2000), near IR emission detected in Gemini/Near-Infrared Integrated Field Spectrograph (NIFS) observations revealed that there is considerable material outside the optical emission-line bicone (Storchi-Bergmann et al. 2009). Furthermore, photoionization models of the NLR emission-line gas in both of these objects, as well as the Seyfert 2 galaxies Mrk 3 (Collins et al. 2009) and Mrk 573 (Kraemer et al. 2009) require a contribution from low-ionization gas ionized by a heavily absorbed continuum, hence, outside the NLR mapped in the light of [O III]. If this low-ionization gas is dusty and along our line-of-sight to the NLR, emission lines from within the optical NLR, such as [O III], would be reddened. There is also evidence for dust features in the inner nuclei of Seyfert galaxies, possibly associated with fueling flows (Martini & Pogge 1999; Martini et al. 2003a; Crenshaw et al. 2010a), which would be a strong source of extinction if they crossed our line-of-sight to the NLR.

Although optical emission-lines, such as [O III] $\lambda 5007$, may be reddened by gas outside the NLR, mid-IR emission lines such as [O IV] $25.89 \mu\text{m}$ will be much less affected. In comparing the ratio of [O III], from ground-based observations, [O IV] from *Spitzer*/IRS spectra, among the 9-month sample of AGN detected by the *Swift*/Burst Alert Telescope (BAT) (Tueller et al. 2008), Meléndez et al. (2008a) found that Seyfert 2s had relatively weaker [O III] than Seyfert 1s², consistent with an $N_H \approx 1-10 \times 10^{21} \text{ cm}^{-2}$. This effect

¹The concept of a screen is an idealization, with the more likely scenario being that the dust is in the plane of the host galaxy or in the form of dusty nuclear spirals. Note, all quoted column densities in this paper are for the simple case of uniform screen, external to the NLR.

²Although weak [O III] could be an indication that ionizing photons are absorbed before they reach the NLR, as suggested by Trouille & Barger (2010), in such a scenario the [O IV] should be similarly affected, which is not typically the case (although see discussion in Weaver et al. [2010]).

was confirmed by Diamond-Stanic, Rieke, & Rigby (2009) and by Baum et al. (2010), using Seyferts in the revised Shapley-Ames, comprised of sources from Maiolino & Rieke (1995) and Ho, Filippenko, & Sargent (1997), and $12\mu\text{m}$ (Rush, Malkan, & Spinoglio 1993) samples, respectively. Diamond-Stanic et al. note that the effect is present even after correcting the [O III] fluxes using the Balmer decrement, which suggests that there are regions from which the optical emission is essentially undetectable. Baum et al. proposed that the unobservable gas lies behind the molecular torus (see, also Nagao et al. 2001). Dudik et al. (2007) found that the ratio of the [Ne V] $14.3\mu\text{m}/24.3\mu\text{m}$ lines in a number of AGN was below the low density limit, hence consistent with extinction. They also suggest that some fraction of the [Ne V] emission arises from behind the torus. However, based on photoionization models, Meléndez et al. (2008a) determined that the [O IV] emission region was \sim a few 10s of pcs from the AGN for most of the targets in the 9-month BAT sample, which requires that the tori possess very large scale heights. Nevertheless, taking the evidence from the $R_{\text{O}3}$ and the [O III]/[O IV] ratios together, one might conclude that the extinction is heaviest towards the inner regions of the NLR.

One open question is whether the extinction is due to dust associated with the AGN, either the torus or the NLR, or dust in the host galaxy. Keel (1980) found a deficiency of Seyfert 1s in nearly edge-on hosts and suggested that Seyfert galaxies have larger bulges or thicker disks than normal spiral galaxies. Maiolino & Rieke (1995) found more Seyfert 1.8s and 1.9s in edge-on systems, hence the reddening of emission from the BLR, which would suppress the broad Balmer lines, could be due to dust in the plane of the host galaxy. Schmitt et al. (2001) also noted a lack of Seyfert 1s in edge-on systems. Hence, one aim of this paper is to isolate the effect of reddening due to gas associated with the AGN, rather than within the plane of the host galaxy. Beyond that, we will determine how much of the [O III] emission is undetected in Seyfert 2s, and, finally, constrain the column densities of the gas outside the optical emission line bicone.

2. Sample Selection and the Effect of Inclination

In order to determine if there are significant differences in the [O III]/[O IV] ratios of Seyfert galaxies, we require a sample that includes a sufficient number of Seyfert 1s and 2s that our results are not biased, e.g., by small number statistics. To begin with, we included AGN for the revised Shapley-Ames sample with IRS spectra analyzed by Diamond-Stanic et al. (2009) and from the $12\mu\text{m}$ sample, with IRS spectra analyzed by Tomassini et al. (2008, 2010). Since both of these samples are weighted towards Seyfert 2s, we added sources from the 22-month BAT sample (Tueller et al. 2010) with IRS spectra analyzed by Meléndez et

al. (in preparation). We stress the point that this is not intended to be a complete, unbiased sample. However, as we will show, the range in $[\text{O III}]/[\text{O IV}]$ ratios and the dependence of this ratio on Seyfert classification is similar to that observed in other studies.

One goal of this study is to isolate the effects of dust associated with the host galaxy from that associated with the NLR. The first step was to eliminate from our sample merging systems and those designated as residing in peculiar host galaxies, based on the galaxy morphologies from the RC3.9 (de Vaucouleurs et al. 1991). The remaining AGN include: 53 Seyfert 2s, 30 Seyfert 1s, 15 Seyfert 1.8/1.9s (“intermediate” Seyferts), and 8 LINERs (see Tables 1 – 4). The uncertainties in the $[\text{O IV}]$ fluxes are found in the references cited in the tables, but are generally $\sim 10\%$. While uncertainties in the $[\text{O III}]$ fluxes are rarely given, Peterson et al. (1991) find that seeing variations in typical ground-based spectroscopy of AGN can result in photometric errors as large as 20%. We therefore assume that our $[\text{O III}]$ fluxes are uncertain at this level. In Figure 1, we show the $[\text{O III}]/[\text{O IV}]$ ratio as a function of the $[\text{O IV}]$ luminosity, which can be used as a proxy for the intrinsic luminosity of the AGN (Meléndez et al. 2008a; Meléndez, Kraemer, & Schmitt 2010). As the plot shows, the sample smoothly spans more than four orders of magnitude in luminosity, hence we do not appear to be introducing obvious biases by including sources from different parent samples (in particular, those from the BAT sample, which includes more distant and luminous sources, see Meléndez et al. [2008a]). It does appear, however, that lower luminosity objects, primarily LINERs, have somewhat higher $[\text{O III}]/[\text{O IV}]$ ratios. As discussed in Netzer (2009), since the AGN in LINERs are weak, they cannot produce as much O^{+3} as Seyferts. Furthermore, starlight may be the dominant form of ionization in LINERs (Cid Fernandes et al. 2009), which would also result in higher $[\text{O III}]/[\text{O IV}]$ ratios. Indeed, the one Seyfert 1 in the low-ionization, high $[\text{O III}]/[\text{O IV}]$ region, Mrk 352, has $[\text{Ne II}] 12.81\mu\text{m}/[\text{Ne III}] 15.56\mu\text{m} \sim 1.6$ (Weaver et al. 2010), indicative of strong star formation (e.g., Meléndez et al. 2008b), which could enhance $[\text{O III}]$.

From their study of *Spitzer*/IRS spectra of Seyfert galaxies, Deo et al. (2007) found that the few objects in their sample that showed deep $10\mu\text{m}$ silicate absorption were in highly inclined or merging systems. Crenshaw & Kraemer (2001) determined that the UV continuum reddening in Seyfert 1s increases dramatically with the inclination of the host galaxy. This suggests that much of the extinction is due to dust the plane of the host galaxy. In Figure 2 we show the effect of inclination in the sample by plotting the $[\text{O III}]/[\text{O IV}]$ ratios versus the axial ratios (b/a) of their host galaxies. Following Crenshaw & Kraemer (2001), we have taken b/a from (in order of preference) de Zotti & Gaskell (1985), Kirhakos & Steiner (1990), and the NASA/IPAC Extragalactic Database (NED) (see Tables 1–4). While there is no strong correlation between $[\text{O III}]/[\text{O IV}]$ and b/a for the sample, there are clearly relatively fewer sources with $[\text{O III}]/[\text{O IV}]$ greater than unity in inclined host

galaxies. Therefore, in examining the effect of extinction associated with the NLR, we opt to only consider those Seyfert galaxies in our sample in hosts with $b/a > 0.5$ (see, also, discussion in Crenshaw & Kraemer 2001). Our final sample includes 40 Seyfert 2s and 26 Seyfert 1s. In Figure 2, one can clearly see that Seyfert 1s, on average, have higher [O III]/[O IV] ratios than do Seyfert 2s. Due to the ionization effect discussed above, we do not include LINERs in the analysis. Intermediate Seyferts exhibit a range of properties (e.g. Goodrich 1995; Trippe et al. 2010), including cases of weak AGN/strong starformation, that can affect [O III] independent from extinction, hence we also exclude these from the analysis of the [O III]/[O IV] ratios. However, they are included in our comparison with R_{O3} and soft X-ray emission (see Section 4).

One possible complication in comparing [O IV] fluxes from *Spitzer* with [O III] fluxes from ground-based observations is the aperture effect. For example, some Seyfert galaxies show [O III] emission from an extended narrow line region (ENLR) up to several kpc from the central source, (e.g. Pogge 1989). For an object at a distance of 10 Mpc, the approximate minimum distance to the Seyfert 1 and 2s in the sample, 1 kpc corresponds to $\sim 20''$, which could be outside the IRS long-low or long-high apertures, with shorter dimensions of $10''.5$ and $11''.1$, respectively (Houck et al. 2004), depending on the orientation of the slit. However, as noted above, based on photoionization models, Meléndez et al. (2008a) determined that the bulk of the [O IV] emission arises close to the AGN, hence it is unlikely that the IRS spectra have missed much of the flux. On the other hand, the [O III] fluxes used here come from a number of different ground-based observers (see Tables 1–4), who employed slits of various dimensions. Nevertheless, as demonstrated by Schmitt et al. (2003b), the [O III] profiles obtained *HST*/Wide Field and Planetary Camera 2 narrow-band images of Seyfert galaxies were strongly centrally peaked and, in most cases, there was a good agreement between the *HST* [O III] fluxes and values from ground-based observations (see their Figure 2). However, it is instructive to examine cases of nearby Seyferts with bright ENLRs. For example, in Figure 3, we show the radial profile of [O III] $\lambda 5007$, derived from a *HST*/STIS slitless G430M spectrum of NGC 4151. In this case, the bulk of the [O III] lies within $\sim 2''$ of the central peak, hence it is reasonably certain that the ground-based observation by Ho et al. (1997), using a $2'' \times 4''$ aperture, captured most of the [O III] flux. For NGC 1068, the [O III] flux measured by Schmitt et al. (2003b), within $4''$ of the AGN, is $\sim 60\%$ of the value obtained by Bonatto & Pastoriza (1997) through a $12''.5 \times 3''.2$ aperture, again indicating that the emission is centrally peaked. Given that these two NLRs are close and extended, it is unlikely that aperture effects play a major role for the other AGN in our sample. As another check, if there is, in general, significant [O III] from the ENLR, one may expect a trend towards higher [O III]/[O IV] ratios with distance. However, as seen in Figure 4, the [O III]/[O IV] ratio is not correlated with distance, which confirms that there is no overall

aperture effect within the sample.

3. Comparison of the [O III]/[O IV] Ratios

As mentioned above, several studies have noted that Seyfert 2s have, on average, lower [O III]/[O IV] ratios than Seyfert 1s, which is attributed to greater extinction towards the NLR in the former. With our reduced sample, we have attempted to account for the effects of peculiar morphologies or host galaxy inclination. In Figure 5, we show the distribution of the ratio for the Seyfert 1s and 2s in the reduced sample, and the separation of the two classes is quite apparent.

The number of objects in our reduced sample is marginally sufficient for a Kolmogorov-Smirnov (K-S) test to return meaningful results. The K-S test yields a D -statistic = 0.55 and a probability of the null hypothesis $p = 8.9 \times 10^{-5}$, indicating that the two populations are different. A two-dimensional Kuiper test of our reduced sample returns $D = 0.525$ and $p = 2.8 \times 10^{-3}$, confirming the result of the K-S test.

The mean [O III]/[O IV] for the Seyfert 1s (excluding Mrk 352, see above) is 2.01, with a 95% confidence interval for the mean of 1.43 – 2.58. For the Seyfert 2s, the mean is 0.97 with a 95% confidence interval of 0.60 – 1.26. The ratio of the means is roughly the same found by LaMassa et al. (2010) in comparing Seyfert 2s from SDSS to Seyfert 1s in the revised Shapley-Ames sample (Diamond-Stanic et al. 2009). In order to determine the average excess extinction in Seyfert 2s, we compared the [O III]/[O IV] ratios for each object to the mean value for the Seyfert 1s. We assumed $R_v = 3.1$, the extinction law of Cardelli, Clayton, & Mathis (1989), and a dust-to-gas ratio resulting in $E(B - V) = 1$ for $N_H = 5.2 \times 10^{21} \text{ cm}^{-2}$ (Shull & van Steenberg 1985). There were four Seyfert 2s with ratios greater than the mean value for the Seyfert 1s, namely, MCG–03–58–7, Tol 1238–364, NGC 1358 and NGC 4507, so we did not include these sources in estimating the extinction; we list the estimates for N_H for the rest in Table 5. For the Seyfert 2s, we find an average reddening of 0.41 ± 0.27 mag, with the 95% confidence interval of 0.32 – 0.50. The mean value for $N_H = 2.1 \times 10^{21} \text{ cm}^{-2}$, with the 95% confidence interval of $1.6 - 2.6 \times 10^{21} \text{ cm}^{-2}$. The range is somewhat smaller than that found by Meléndez et al. (2008a), which is likely due to the rejection of Seyferts in inclined hosts.

One caveat regarding estimates of reddening based on the [O III]/[O IV] ratios is that it is likely, when the host galaxy is viewed at low inclination, that half of the NLR emission lies behind the galactic disk (e.g. Crenshaw et al. 2010b; Fischer et al. 2010). Therefore, depending on the amount of dust in the disk, there can be significant extinction of the

[O III]. Interestingly, Mrk 3 resides in an S0 host galaxy (de Vaucouleurs et al., 1991), hence its relatively large [O III]/[O IV] ratio of 1.62 may be in part due lack of dust in the galactic disk.

Intermediate Seyferts exhibit weak Balmer lines either due to the inherent weakness of the BLR emission, reddening of the BLR, or a combination of these effects (e.g. Trippe et al. 2010). If the extinction also affects the NLR, they might be expected to have [O III]/[O IV] ratios similar to Seyfert 2s. In our sample, there is one clear outlier, NGC 3982, with an [O III]/[O IV] = 10.0, which is likely affected by a strong contribution from star formation (Meléndez et al. 2008b). Dropping NGC 3982, the mean [O III]/[O IV] for the intermediate Seyferts is 1.24, with a 95% confidence interval of 0.38 – 2.10. A K-S test comparing this ratio for intermediate Seyferts with that for Seyfert 1s yields $D = 0.36$ and $p = 0.25$, while comparing them with Seyfert 2s yields $D = 0.20$ and $p = 0.87$. Hence, based on the [O III]/[O IV] ratios, intermediate Seyferts straddle the range of extinction among the Seyfert 1s and 2s. While there are too few LINERs in our sample to perform a K-S test, their mean [O III]/[O IV] is 4.79, which is consistent with their weak AGN and lower-ionization NLRs .

4. Comparison with other Emission Lines

4.1. The R_{O3} and Obscuration of the Inner NLR

As mentioned in Section 1, Nagao et al. (2001) suggested that the lower values of R_{O3} in Seyfert 2s were due to the obscuration of high density/high emissivity gas in the inner NLR, which they characterized with $n_H = 10^7 \text{ cm}^{-3}$. They further suggested that the differences in R_{O3} 's between Seyfert 1s and 2s could be explained by a 5–20% contribution from this component in the former compared to a 0–5% contribution in the latter. Similarly, in order to match the R_{O3} observed in the bright, central emission-line knot in NGC 4151, we (Crenshaw & Kraemer 2005) generated a multi-component photoionization model, with the [O III] $\lambda 4363$ emission dominated by gas with $n_H = 10^{6.2} \text{ cm}^{-3}$, at a distance of $\sim 2 \text{ pc}$ from the central source.

In Figure 6, we plot R_{O3} against [O III]/[O IV] (given the small number of sources for which R_{O3} 's have been published, we included Seyferts in inclined hosts). There is no apparent correlation, with a Spearman rank coefficient of 0.14 and significance of deviation from zero of 0.39. However, by over-plotting R_{O3} for 20,000K in the low density limit (Osterbrock & Ferland 2006) and the mean [O III]/[O IV] for the Seyfert 1s in our sample, one can see there are 4 distinct quadrants. Most of the Seyfert 1s lie in the upper two

quadrants, indicating a contribution from dense gas to the R_{O3} . There are 9 Seyfert 1s in the upper left, with $[O\ III]/[O\ IV]$ below the the minimum value of the 95% confidence interval. For several of these, the weak $[O\ III]$ could be due to reddening by an external dust that covers the NLR, as is likely the case for NGC 4235, which is inclined, and, possibly, for NGC 6814, MCG–6–30–15, and ESO 140–G043 which have reddened continua (Morris & Ward 1988). On the other hand, most (12/19) of the Seyfert 2s lie in the lower left quadrant. We interpret this as an indication that the extinction is greatest towards the inner NLR, which includes the dense $[O\ III]$ -emitting gas (but, see discussion in Section 5.). Note that there are a number of Seyfert 2s that have $[O\ III]/[O\ IV]$ similar to the (presumably) reddened Seyfert 1s, yet have lower R_{O3} , which is consistent with dust surrounding the inner NLR in the former versus a more uniform external screen in the latter. There is some overlap between the two classes near the middle of the diagram, which could be a result of a relatively weak contribution from the dense component in some Seyfert 1s and/or less extinction towards the inner NLR in some Seyfert 2s, which, in turn, may be the an indication of patchy dust that allows a more direct view of the dense component.

There are a few odd points in Figure 6. Two Seyfert 2s lie in the upper right quadrant: NGC 424 and NGC 1358, The former has also been classified as an intermediate Seyfert (Murayama, Taniguchi, & Iwasawa 1998), hence it is not necessarily surprising that it has properties in common with Seyfert 1s. Although Nagao et al.(2001) list an R_{O3} for NGC 1358 based on emission line ratios from Phillips, Charles, & Baldwin (1983), neither Ho, Filippenko, & Sargent (1995) nor Vaceli et al. (1997) reported a detection of $[O\ III]\ \lambda 4363$, therefore, R_{O3} is uncertain. The one intermediate Seyfert, NGC 7314, is found in the lower left quadrant. However, it is has a $b/a = 0.43$, hence there is likely to be extinction due to dust in the plane. Among the Seyfert 1s, the very low R_{O3} for Mrk 6 may be somewhat suspect, as Nagao et al. averaged values from Koski (1978) and Cohen (1983) and the latter measured relatively stronger 4363 emission. The “prototypical” Seyfert 1 galaxy, NGC 4151, occupies the most extreme position in the lower right quadrant. There is evidence, however, that the extended NLR in NGC 4151 was ionized when the central source was significantly more luminous than at present (e.g.. Schulz & Komossa 1993; Wang et al. 2010). Hence, there may be a relatively large contribution from low density gas which would have the effect of reducing R_{O3} .

4.2. Soft X-ray Emission

High resolution X-ray spectra Seyferts, obtained with *Chandra* (e.g., Sako et al. 2000; Ogle et al. 2000) and *XMM-Newton* (e.g. Kinkhabwala et al. 2002), have revealed the

presence of numerous soft X-ray (energies < 2 keV) emission lines. Based on *Chandra*/ACIS imaging, the X-ray emission line region appears to be roughly coincident with the [O III] emission (Sako et al.2000; Ogle et al. 2000; Zeng 2009), and it is probable that both the X-ray and optical emission line gas are photoionized by the central source (Bianchi, Guainazzi, & Chiaberge 2006). The strongest emission line in the soft X-ray spectra of Seyfert galaxies is typically the forbidden line ($1s^2^1S_0 - 1s2s^3S_1$) of He-like oxygen, O VII-f 22.1Å . If the NLR is surrounded by dusty gas, which reddens the [O III], one would expect that the same gas would absorb the O VII.

We have X-ray fluxes for 15 sources, obtained from *XMM-Newton*/reflection grating spectrometer (RGS) data (see Table 6). Those fluxes listed as from “this paper” are from the set of archival RGS spectra analyzed by Guainazzi & Bianchi (2007); the details of the spectral analysis are described therein. Due to the small number of sources for which OVII-f line fluxes available, we have added NGC 424, NGC 7582, NGC 3227, which are in inclined hosts, and NGC 2992, which was left out of the [O III]/[O IV] comparison since it is in a peculiar host galaxy. In Figure 7, we show the flux ratios O VII-f/[O IV] versus those of [O III]/[O IV]. There is a clear trend, although with the caveat that the sample size is small, with a Spearman rank coefficient of 0.736 and significance of deviation from zero of 0.0008. The more reddened sources, as indicated by the smaller [O III]/[O IV] ratios show relatively weaker O VII.

We determined the additional column density towards the X-ray emission region in the Seyfert 2s and intermediate Seyferts by, first, running a series of models with XSPEC 12 (Arnaud 1996), using tbabs, the Tuebingen-Boulder ISM absorption for the absorption model (Wilms, Allen and McCray 2000), an O VII line width $\sigma = 3$ eV and assuming the line is observed at the emitted energy, in order to obtain the ratios of observed line strength to the intrinsic line strength as a function of N_H . Then, we determined N_H for the individual sources by matching the ratio of the observed O VII-f/[O IV] to the mean value for the Seyfert 1s, O VII-f/[O IV] = 0.31, to the computed observed/emitted ratio. The values are listed in Table 5. In 7/10 sources, the X-ray column is either on the same order or somewhat smaller than the column of dusty gas. The latter can occur if the absorber is ionized, hence the derived X-ray column would be a lower limit. For Mrk 3 and MCG–03–34–64, the X-ray column is significantly larger than the dusty column. As noted in Section 3., Mrk 3 may have a lower ISM dust-to-gas than in the Galactic ISM. MCG–03–34–64 shows evidence of Wolf-Rayet stars (Cid Fernandes et al. 2004), indicative of a young stellar population, which may strengthen [O III] relative to [O IV], hence making the [O III]/[O IV] ratio a less reliable indicator of dust towards the NLR. NGC 424 has [O III]/[O IV] greater than the Seyfert 1 mean, in keeping with the possibility of a direct view of the inner NLR (e.g. Murayama et al. 1998), however its O VII-f/[O IV] ratio indicates significant absorption.

One possibility is that much of the O VII forms closer to the AGN than the [O III] (see discussion in Iwasawa et al. 2001) and is absorbed by gas that does not cover a significant portion of the inner NLR. Or, it may simply be that the gas external to the inner NLR of NGC 424 has a low dust-to-gas ratio.

Based on photoionization modeling of RGS spectra of NGC 3516 (Turner et al. 2003) and NGC 4151 (Armentrout et al. 2007), there is evidence that the soft X-ray emission line gas has similar properties, in terms of ionization state and column density, to those of warm absorbers (e.g., Crenshaw, Kraemer, & George 2003). Since the warm absorbers may originate as part of a disk wind (Kraemer et al. 2005; Krongold et al. 2007, 2010; Turner et al. 2008), which may expand and dissipate unless confined, it is possible that the associated emission is centrally peaked, as suggested in the case of NGC 424. If the lower R_{O3} 's detected in Seyfert 2s are indicative of greater extinction towards the inner NLR, one might expect a correlation between the R_{O3} and the O VII-f/[O IV] ratios. However, for the eleven objects for which we have both [O III] $\lambda 4363$ and O VII-f fluxes, we obtain a Spearman rank coefficient of 0.49 and significance of deviation from zero of 0.13, thus there is no strong evidence for a correlation. This suggests that, unlike [O III] $\lambda 4363$, the soft X-ray emission is not typically centrally peaked, although there are too few data points to make any definite conclusions.

5. Distribution of Dusty Gas External to the NLR

The lower [O III]/[O IV], O VII-f/[O IV] and R_{O3} ratios in Seyfert 2s, as compared to Seyfert 1s, are consistent with a line-of-sight through dusty gas outside the optical NLR. The question is how this gas is distributed and, specifically whether it is associated with the torus, (e.g., Nagao et al. 2001; Baum et al. 2010) or dust structure at larger radial distances (e.g, Capetti et al. 1996; Malkan, Gorjian, & Tam 1998; also, see discussion below). Krolik & Begelman (1988) determined that the ratio of the scale height of the torus to its radius is ~ 0.7 . Based on observations of H₂O MASERs, the outer radius is $\sim 2 - 15$ pc (Gallimore et al. 1996; Taniguchi & Murayama 1998), in general agreement with IR interferometric observations of nuclear dust distributions in several nearby Seyferts (Tristram et al. 2007; Raban et al. 2009; Burtscher et al. 2009). Therefore, if emission that arises from larger radial distances is absorbed, it must be by dusty gas more distant than the outer radii determined from the H₂O MASERs.

The correlation between the O VII-f/[O IV] and [O III]/[O IV] ratios is generally consistent with a scenario in which the O VII and [O III] regions are 1) co-located and 2) viewed through the same dusty gas in Seyfert 2 galaxies, but it does not lead to clear constraints

on the distribution of the external gas. Based on our modeling of NGC 4151 (Crenshaw & Kraemer 2005), assuming a density law $n_H \propto r^{-1.7}$ (Kraemer et al. 2000), the radial distance at which n_H falls to $10^{4.8} \text{ cm}^{-3}$, or an order of magnitude below the critical density for de-excitation of the 1D_2 level of O III (Osterbrock & Ferland 2006), is ~ 13 pc. Hence, it is plausible that the dense O III-emitting component could be hidden if our view of NGC 4151 intersected the torus, as in Seyfert 2s. The radial profile of [O III] $\lambda 5007$, Figure 3, provides additional constraints on the distribution of the dust (for the details on the analysis, see Crenshaw & Kraemer 2005). The emission is centrally peaked, as seen in other Seyfert 1s (e.g., Schmitt et al. 2003a), but only $\sim 30\%$ of the total [O III] comes from within ~ 30 pc of the central source. Therefore, even the complete extinction of this component would be insufficient to account for the difference in the [O III]/[O IV] ratios of Seyfert 1s and 2s. If Seyfert 2 galaxies have similar intrinsic [O III] profiles, the dust must extend further out along the NLR.

One way to test if the external dust is thickest towards the apex of the bicone is to compare the extinction of the dense [O III] component with the overall extinction of [O III] $\lambda 5007$. Based on Nagao et al. (2001), the differences in the contribution of the dense component in Seyfert 1s and 2s typically requires $\sim 80\%$ suppression of [O III] $\lambda 4363$ in the latter. For an ISM extinction curve and dust-to-gas ratio, this corresponds to an $N_H \approx 2.2 \times 10^{21} \text{ cm}^{-2}$, which is within the 95% confidence interval for N_H computed from the [O III]/[O IV] ratios (see Section 3). If the [O III] $\lambda 5007$ is extended, as the STIS spectrum of NGC 4151 indicates, this suggests that the dust is not centrally peaked, but, rather, extends further along the NLR. Also, based on photoionization modeling of STIS longslit spectra of the Seyfert 2 galaxies NGC 1068 (Kraemer & Crenshaw 2000b), Mrk 3 (Collins et al. 2009), and Mrk 573 (Kraemer et al. 2009), we have found that the innermost optically-detected emission to be 10's of parsecs from the AGN, which is consistent with extended dust structure.

Malkan et al. (1998) found evidence for excess galactic dust in Seyfert 2 galaxies, at radial distance of up to several 100s of pc, which could obscure the BLR and central continuum. They attributed the absence of such structures in Seyfert 1s as due to differences in the host galaxy properties. However, de Zotti & Gaskell (1985) suggested that gas associated with the host galaxy is evacuated out to distances of $\lesssim 100$ pc, presumably due to the effect of radiation pressure and/or winds from the AGN. As discussed in Crenshaw & Kraemer (2001), such a scenario would lead to differences in reddening as a function of viewing angle towards the AGN. When one's line-of-sight is close to the bicone axis, i.e. when viewing the object as a Seyfert 1, there is little extinction. However, when the bicone axis is closer to the plane of the sky, i.e., when the object is seen as Seyfert 2, the intervening gas has been less affected by the AGN, hence the extinction can be significant. The fact that there is evidence

for dust external to the optical NLR in NGC 1068 (Kraemer & Crenshaw 2000a), but not in the case of NGC 4151 (Kraemer et al. 2000), is consistent with this scenario. Furthermore, Capetti et al. (1996) estimate a scale height of ~ 180 pc for the dust lane crossing the nucleus in the Seyfert 2 galaxy Mrk 78. In summary, there is evidence that obscuring dust extends far along the NLR. Models of extended (e.g., Garanato, Danese, & Franceschini 1997) or clumpy tori (Nenkova, Ivezić, & Elitzur 2002) suggest that associated dust structure may extend ~ 100 pc. Another possibility is that the dust structure is associated with nuclear dust spirals (Regan & Mulchaey 1999; Pogge & Martini 2002; Martini et al. 2003b), which, in turn may be part of the fueling flow to the AGN (Martini et al. 2003a; Deo, Crenshaw, & Kraemer 2006; Simões Lopes et al. 2007).

6. Summary

We have selected 108 AGN from the RSA, $12\mu\text{m}$, and BAT samples, after rejecting those in peculiar host galaxies, to study the effects of extinction and absorption towards the NLR. First, we compared ground-based [O III] $\lambda 5007$ fluxes, taken from the literature, with [O IV] $25.89\mu\text{m}$ fluxes from *Spitzer*/IRS observations. Using [O IV] as a proxy for bolometric luminosity, we find evidence for larger [O III]/[O IV] in the least luminous sources, which we suggest is an ionization affect (e.g., Netzer 2009). We also find that AGN in host galaxies with $b/a < 0.5$ tend to have lower [O III]/[O IV] ratios, which we attribute to extinction by dust in the plane of the host galaxy. After eliminating the inclined objects from our sample, we were left with 40 Seyfert 2s and 26 Seyfert 1s. We find the following:

1. In the reduced sample, the [O III]/[O IV] ratio is lower, with statistical significance, in Seyfert 2s than Seyfert 1s, which is consistent with the NLR in Seyfert 2s being viewed through an additional column of dusty gas with $N_H \sim 2 \times 10^{21} \text{ cm}^{-2}$. Although the relative weakness of [O III] in Seyfert 2s has been noted previously (e.g., Meléndez et al. 2008a; Diamond-Stanic et al. 2009; Baum et al. 2010, Lamassa et al. 2010), this is first time the effect has been demonstrated after accounting for possible effects from the host galaxy. We find that intermediate Seyferts have [O III]/[O IV] ratios spanning the range seen in Seyfert 1s and 2s, which suggests that some may have weak BLR emission due to reddening while others may possess weak AGN, hence intrinsically weak BLR emission (see Trippe et al. 2010).

2. We compared the [O III]/[O IV] ratios to R_{O_3} , for a subset of the sample for which [O III] $\lambda 4363$ measurements were available: 20 Seyfert 2s, 21 Seyfert 1s, and 2 intermediate Seyferts. Seyfert 2s were generally found to have both low [O III]/[O IV] ratios and R_{O_3} below the low-density limit for gas at 20,000K. As shown by Nagao et al. (2001), most

Seyfert 1s have R_{O3} above the low-density limit, consistent with a contribution from gas with $n_H > 10^6 \text{ cm}^{-3}$, which is likely within $\sim 15 \text{ pc}$ of the central source (e.g. Crenshaw & Kraemer 2005). If extinction reduces the contribution to $[O \text{ III}] \lambda 4363$ from the dense component by 80% in the Seyfert 2s, as suggested by Nagao et al., this region would be viewed though dusty gas with column density similar to the mean value derived from the $[O \text{ III}]/[O \text{ IV}]$ ratios.

3. Limited by the availability of high-resolution X-ray spectra, we were able to compare the ratios of $O \text{ VII-f}/[O \text{ IV}]$ and $[O \text{ III}]/[O \text{ IV}]$ for 17 Seyfert in our sample. We find a correlation between the ratios, which is expected given the evidence that $O \text{ VII-f}$ and $[O \text{ III}]$ regions are co-located (e.g. Zeng 2009). We estimated the amount of intervening material required to account for the absorption of the $O \text{ VII}$ emission in Seyfert 2s and find, with a few exceptions, that the X-ray absorbing column density are roughly on the same order as those of the dusty gas. While lower X-ray predicted column densities, compared to dusty columns, may indicate that the absorbers are partially ionized, the higher X-ray predicted columns are more consistent with low dust-to-gas ratios in the absorbers.

4. Using a STIS G430M slitless spectrum of NGC 4151, we determined that only $\sim 30\%$ of the $[O \text{ III}] \lambda 5007$ comes from the inner $\sim 30 \text{ pc}$. If Seyfert 2s have similar intrinsic $[O \text{ III}]$ profiles, the dust must extend to larger radial distances. Based on this and the results of our previous photoionization modeling of Seyfert 2 galaxies, we suggest that dusty gas surrounds the NLR and extends out to radial distances of at least 10s of parsecs. Based on scale-height constraints for torus models, the obscuring gas must lie further from the AGN than the maximum radial distance estimated from H_2O MASERs. One possibility is this gas is associated with the nuclear dust spirals observed in many Seyferts. In any case, it points to the presence of a significant amount of material outside the optical NLR, in agreement with results from NIFS spectra of a several Seyfert galaxies (Riffel et al. 2008; Storchi-Bergmann et al. 2009; Riffel, Storchi-Bergmann, & Nagar 2010).

Basic research in Astronomy at the NRL is supported by 6.1 base funding. This research has made use of the NASA/IPAC Extragalactic Database (NED) which is operated by the Jet Propulsion Laboratory, California Institute of Technology, under contract with the National Aeronautics and Space Administration. We thank Juliette Buet for her assistance with this project. We thank an anonymous referee for valuable suggestions.

REFERENCES

Antonucci, R.R.J. 1993, ARA&A, 31, 473

- Armentrout, B.K., Kraemer, S.B., & Turner, T.J. 2007, *ApJ*, 665, 237
- Arnaud, K. 1996, *Astronomical Data Analysis Software and Systems V*, ed. G.H. Jacoby & J. Barnes, ASP Conf. Ser., 101, 17
- Baum, S.A., et al. 2010, *ApJ*, 710, 289
- Bianchi, S., Guainazzi, M., & Chiaberge, M. 2006, *A&A*, 448, 499
- Bonatto, C.J., & Pastroiza, M.G. 1997, *ApJ*, 486, 132
- Burtscher, L., Jaffe, W., Rban, D., Meisenheimer, K., Tristram, K.R.W., & Röttgering, H. 2009, *ApJ*, 705, L53
- Capetti, A., Axon, D.J., Macchetto, F., Sparks, W.B., Boksenberg, A. 1996, *ApJ*, 469, 554
- Cardelli, J.A., Clayton, G.C., & Mathis, J.S. 1989, *ApJ*, 345, 245
- Cid Fernandes, R., Gu, Q., Melnick, J., Terlevich, E., Terlevich, R., Kunth, D., Rodrigues Lacerda, R., & Joguet, B. 2004, *MNRAS*, 355, 273
- Cid Fernandes, R., Heckman, T., Schmitt, H., González Delgado, R. M., & Storchi-Bergmann, T. 2001, *ApJ*, 558, 81
- Cid Fernandes, R., Stasińska, G., Vale Asari, N., Mateus, A., Schlickmann, M.S. & Schoenell, W. 2010, in *Co-Evolution of Central Black Holes and Galaxies*, Proc. of the International Astronomical Union, IAU Symposium, 267, 65
- Cohen, R.D. 1983, *ApJ*, 273, 489
- Collins, N.R., Kraemer, S.B., Crenshaw, D.M., Bruhweiler, F.C, & Meléndez, M. 2009, *ApJ*, 694, 765
- Crenshaw, D.M., & Kraemer, S.B. 2001, *ApJ*, 562, L29
- Crenshaw, D.M., & Kraemer, S.B. 2005, *ApJ*, 625, 680
- Crenshaw, D.M., Kraemer, S.B., & George, I.M. 2003, *ARA&A*, 41, 117
- Crenshaw, D.M., Kraemer, S.B., Schmitt, H.R., Jaffé, Y.L., Deo, R.P., Collins, N.R., & Fischer, T.C. 2010a, *AJ*, 139, 871
- Crenshaw, D.M., Schmitt, H.R., Kraemer, S.B., Mushotzky, R.F., & Dunn, J.P. 2010b, *ApJ*, 708, 419
- Deo, R.P., Crenshaw, D.M., & Kraemer, S.B. 2006, *AJ*, 132, 321
- Deo, R.P., Crenshaw, D.M., Kraemer, S.B., Dietrich, M., Elitzur, M., Teplitz, H., & Turner, T.J. 2007, *ApJ*, 671, 124
- de Robertis, M.M., & Osterbrock, D.E. 1986, *ApJ*, 301, 98

- de Vaucouleurs, G., de Vaucouleurs, A., Corwin, H.G., Buta, R.J., Paturel, G., & Fouqué, P. 1991, *Third Reference Catalogue of Bright Galaxies*, (New York, NY: Springer)
- de Zotti, G., & Gaskell, C.M. 1985, *A&A*, 147, 1
- Diamond-Stanic, A.M., Rieke, G.H., & Rigby, J.R. 2009, *ApJ*, 698, 623
- Dudik, R.P., Weingartner, J.C., Satyapal, S., Fischer, J., Dudley, C.C., O’Halloran, B. 2007, *ApJ*, 664, 71
- Ferland, G.J., & Osterbrock, D.E. 1986, *ApJ*, 300, 658
- Filippenko, A.V., & Halpern, J.P. 1984, *pJ*, 285, 458
- Fischer, T.C., Crenshaw, D.M., Kraemer, S.B., Schmitt, H.R., & Trippe, M.L. 2010, *AJ*, 140, 577
- Gallimore, J.F., Baum, S.A., O’Dea, C.P., Brinks, E., & Pedlar, A. 1996, *ApJ*, 462, 740
- Goodrich, R.W. 1995, *ApJ*, 440, 141
- Goodrich, R.W., & Osterbrock, D.E. 1983, *ApJ*, 269, 416
- Granato, G., Danese, L., Franceschini, A. 1997, *ApJ*, 486, 147
- Guainazzi, M., & Bianchi, S. 2007, *MNRAS*, 374, 1290
- Gu, Q., Melnick, J., Cid Fernandes, R., Kunth, D., Terlevich, E., & Terlevich, R. 2006, *MNRAS*, 366, 480
- Ho, L.C., Filippenko, A.V., & Sargent, W.L.W. 1997, *ApJ*, 487, 579
- Ho, L.C., Filippenko, A.V., & Sargent, W.L.W. 1995, *ApJS*, 98, 477
- Houck, J.R., et al. 2004, *ApJS*, 154, 18
- Iwasawa, K., Matt, G., Fabian, A.C., Bianchi, S., Brandt, W.N., Guainazzi, M., Murayama, T., & Taniguchi, Y. 2001, *MNRAS*, 326, 119
- Kaspi, S., et al. 2002, *ApJ*, 574, 642
- Keel, W.C. 1980, *AJ*, 85, 198
- Khackikian, E.Y., & Weedman, D.W. 1974, *ApJ*, 581
- Kinkhabwala, A., Sako, M., Behar, E., Kahn, S.M., Paerels, F., Brinkman, A.C., Kaastra, J.S., Gu, M.F., & Liedahl, D.A. 2002, *ApJ*, 575, 732
- Kirhakos, S.D., & Steiner, J.E. 1990, *AJ*, 99, 1435
- Königl, A., & Kartje, J.F. 1994, *APJ*, 434, 446
- Koski, A.T. 1978, *ApJ*, 223, 56
- Kraemer, S.B. & Crenshaw, D.M. 2000a, *ApJ*, 544, 763

- Kraemer, S.B., & Crenshaw, D.M. 2000b, *ApJ*, 532, 53
- Kraemer, S.B., Crenshaw, D.M., Hutchings, J.B., Gull, T.R., Kaiser, M.E., Nelson, C.H., & Weistrop, D. 2000, *ApJ*, 531, 278
- Kraemer, S.B., Trippe, M.L., Crenshaw, D.M., Meléndez, M., Schmitt, H.R., & Fischer, T.C. 2009, *ApJ*, 698, 106
- Kraemer, S.B., Wu, C.-C., Crenshaw, D.M., & Harrington, J.P. 1994, *APJ*, 435, 171
- Kraemer, S.B., et al. 2005, *ApJ*, 633, 693
- Krolik, J.H., & Begelman, M.C. 1988, *ApJ*, 329, 702
- Krongold, Y., et al. 2010, *ApJ*, 710, 360
- Krongold, Y., Nicastro, F., Elvis, M., Brickhouse, N., Binette, L., Mathur, S., & Jiménez-Bailón, E. 2007, *ApJ*, 659, 1022
- LaMassa, S.M., Heckman, T. M., Ptak, A., Martins, L., Wild, V., & Sonnentrucker, P. 2010, *ApJ*, 720, 786
- Lutz, D., Sturm, C., Genzel, R., Moowrwood, A.F.M., Alexander, T., Netzer, H., & sternberg, A. 2000, *ApJ*, 536, 697
- MacAlpine, G.M. 1988, *PASP*, 100, 65
- Maiolino, R., & Rieke, G.H. 1995, *ApJ*, 454, 95
- Malkan, M. A., Gorjian, V., & Tam, R. 1998, *ApJS*, 117, 25
- Martini, P., & Pogge, R.W. 1999, *AJ*, 118, 2646
- Martini, P., Regan, M.W., Mulchaey, J.S., & Pogge, R.W. 2003a, *ApJ*, 589, 774
- Martini, P., Regan, M.W., Mulchaey, J.S., & Pogge, R.W. 2003b, *ApJS*, 146, 353
- Meléndez, M. et al. 2008a, *ApJ*, 682, 94
- Meléndez, M., Kraemer, S.B., & Schmitt, H.R. 2010, *MNRAS*, 406, 493
- Meléndez, M., Kraemer, S.B., Schmitt, H.R., Crenshaw, D.M., Deo, R.P., Mushotzky, R.F., & Bruhweiler, F.C. 2008b, *ApJ*. 689, 95
- Miller, J.S., & Antonucci, R.R.J. 1983, *ApJ*, 271, L7
- Morris, S.L., & Ward, M.J. 1988, *MNRAS*, 230, 639
- Mulchaey, J.S. 1994, Ph.D. thesis, University of Maryland, College Park
- Murayama, T., Taniguchi, Y., & Iwasawa, K. 1998, *AJ*, 115, 460
- Nagao, T., Murayama, T., & Taniguchi, Y. 2001, *ApJ*, 549, 155
- Nenkova, M., Ivezić, Z., & Elitzur, M. 2002, *ApJ*, 570, L9

- Netzer, H. 2009, MNRAS, 399, 1907
- Ogle, P.M., Marshall, H. L., Lee, J.C., & Canizares, C.R. 2000, ApJ, 545, L81
- Osterbrock, D.E., & Ferland, G.J. 2006, *Astrophysics of Gaseous Nebulae and Active Galactic Nuclei*, 2nd Ed. (Sausalito, CA: Univ. Science Books)
- Peterson, B.M., et al. 1991, ApJ, 368, 119
- Phillips, M.M., Charles, P.A., Baldwin, J.A. 1983, ApJ, 266, 485
- Pogge, R.W. 1988a, APJ, 332, 702
- Pogge, R.W. 1988b, ApJ, 328, 519
- Pogge, R.W. 1989, ApJ, 345, 730
- Pogge, R.W., & Martini, P. 2002, ApJ, 569, 624
- Raban, D., Jaffe, W., Röttgering, H., Meisenheimer, K., & Tristram, K.R.W. 2009, MNRAS, 394, 1325
- Regan, M.W., & Mulchaey, J.S. 1999, AJ, 117, 2676
- Riffel, R.A., Storchi-Bergmann, T., & Nagar, N.M. 2010, MNRAS, 404, 166
- Riffel, R.A., Storchi-Bergmann, T., Winge, C., McGregor, P.J., Beck, T., & Schmitt, H. 2008, MNRAS, 385, 1129
- Rush, B., Malkan, M. A., & Spinoglio, L. 1993, ApJS, 89, 1
- Sako, M., Kahn, S.M., Paerels, F., & Liedahl, D. A. 2000, ApJ, 543, L115
- Schmitt, H.R., Antonucci, R.R.J., Ulvestad, J.S., Kinney, A.L., Clarke, C.J., & Pringle, J.E. 2001, ApJ, 555, 663
- Schmitt, H.R., & Kinney, A.L. 1996, ApJ, 463, 498
- Schmitt, H.R., Donley, J.L., Antonucci, R.R.J., Hutchings, J.B., Kinney, A.L., & Pringle, J.E. 2003a, ApJ, 597, 768
- Schmitt, H.R., Donley, J.L., Antonucci, R.R.J., Hutchings, J.B., Kinney, A.L. 2003b, ApJS, 148, 327
- Schulz, H., & Komossa, S. 1993, A&A, 278, 29
- Shull, J.M., & van Steenberg, M.E. 1985, ApJ, 294, 599
- Simões Lopes, R.D., Storchi-Bergmann, T., de Fátima Saraiva, M., & Martini, P. 2007, ApJ, 655, 718
- Stauffer, J.R. 1982, ApJ, 262, 66
- Steenbrugge, K.C., et al. 2005, A&A, 434, 569

- Storchi-Bergmann, T., McGregor, P.J., Riffel, R. A., Simões Lopes, R., Beck, T., & Dopita, M. 2009, MNRAS, 394, 1148
- Taniguchi, Y., & Murayama, T. 1998, ApJ, 501, L25
- Tommasin, S., Spinoglio, L., Malkan, M.A., Smith, H., González-Alfonso, E., & Charmandaris, V. 2008, ApJ, 676, 836
- Tommasin, S., Spinoglio, L., Malkan, M.A., & Fazio, G. 2010, ApJ, 709, 1257
- Trippe, M.L., Crenshaw, D.M., Deo, R.P., Dietrich, M., Kraemer, S.B., Rafter, S.E., & Turner, T.J. 2010, submitted to ApJ
- Tristram, K.R.W., et al. 2007, A&A, 474, 837
- Tueller, J., Mushotzky, R.F., Barthelmy, S., Cannizzo, J.K., Gehrels, N., Markwardt, C.B., Skinner, G.K., & Winter, L.M. 2008, ApJ, 681, 113
- Tueller, J. et al. 2010, ApJS, 186, 378
- Turner, T.J., Kraemer, S.B., Mushotzky, R.F., George, I.M., & Gabel, J.R. 2003, ApJ, 594, 128
- Turner, T.J., Reeves, J.N., Kraemer, S.B., & Miller, L. 2008, A&A, 483, 161
- Vaceli, M.S., Viegas, S.M., Gruenwald, R., & de Souza, R.E. 1997, AJ, 114, 1345
- Wang, J. Fabbiano, G., Risaliti, G., Elvis, M., Mundell, C.G., Dumas, G., Schinnerer, E., & Zezas, A. 2010, ApJ, 719, L208
- Weaver, K. A., et al. 2010, ApJ, 716, 1151
- Whittle, M. 1992, ApJS, 79, 49
- Wilms, J., Allen, A., & McCray, R. 2000, ApJ, 542, 914
- Zeng, J. 2009, Ph.D. thesis, University of Maryland, Baltimore County

Fig. 1.— The ratio of $[\text{O III}]\lambda 5007/[\text{O IV}] 25.89\mu\text{m}$ plotted against $[\text{O IV}]$ luminosity, for the complete sample. Symbols are as follows: Seyfert 1s, asterisks; Seyfert 2s, crosses; Intermediate Seyferts, diamonds; LINERs, triangles. Typical uncertainty is shown at the left of the figure. As noted in Section 2, while there is no overall trend, a number of lower luminosity objects have large $[\text{O III}]/[\text{O IV}]$ ratios, which we attribute to an ionization effect.

Fig. 2.— The $[\text{O III}]/[\text{O IV}]$ ratio as a function of inclination (the ratio of the semi-minor to semi-major axis of the host galaxy). Symbols are as in Figure 1, and the typical uncertainty in $[\text{O III}]/[\text{O IV}]$ is shown at the left. Note the relative paucity of sources with $[\text{O III}]/[\text{O IV}]$ greater than unity in hosts with $b/a < 0.5$.

Fig. 3.— Plot of the surface brightness, co-added in the dispersion direction, as a function of distance from the nucleus in the cross-dispersion direction in a STIS/G430M slitless spectrum of NGC 4151. The top profile is continuum plus $[\text{O III}]$ emission, and the bottom profile is just the $[\text{O III}]$ emission, obtained by subtracting the continuum profile from a nearby region.

Fig. 4.— The $[\text{O III}]/[\text{O IV}]$ ratio as a function of distance (distances are mean values from the literature, as listed in NED; if none are available, distances are determined from z , assuming $H_0 = 71 \text{ km s}^{-1} \text{ Mpc}^{-1}$). Symbols as in Figure 1, with the typical uncertainty in $[\text{O III}]/[\text{O IV}]$ shown at left.

Fig. 5.— Histogram showing the $[\text{O III}]/[\text{O IV}]$ ratios for the Seyfert 1s and Seyfert 2s in the reduced sample (see discussion in Sections 2 and 3).

Fig. 6.— Comparison of R_{O3} and $[\text{O III}]/[\text{O IV}]$. Symbols as in Figure 1, except Seyfert 1s are shown in green and Seyfert 2s are shown in red; typical uncertainty in the ratios are shown at left. Several objects discussed in Section 4.1 are identified. The vertical dash-dotted line shows the mean $[\text{O III}]/[\text{O IV}]$ ratio for the Seyfert 1s in the reduced sample, while the horizontal dotted line shows the value of R_{O3} for a 20,000K in the low-density limit.

Fig. 7.— Comparison of the $\text{OVII-f}/[\text{O IV}]$ and $[\text{O III}]/[\text{O IV}]$ ratios. Symbols as in Figure 1. The over-plotted line shows a linear regression fit to the points.

Table 1. Properties of the Seyfert 2 Galaxies in the Sample^a

name	Distance(Mpc) ^b	original sample(s)	F[O IV] ^c	F[OIII] ^c	b/a	logR _{O3}
Mrk 348	63.5	12 μ m, BAT	1.76×10^{-13} ; 1	2.2×10^{-13} ; 2	0.91; 3	-1.77; 4
IRAS 00521–7054	291.0	12 μ m	8.63×10^{-14} ; 1	7.9×10^{-14} ; 2	0.87; 5	
NGC 424	49.7	12 μ m	2.58×10^{-13} ; 6	7.5×10^{-13} ; 2	0.36; 3	-1.30; 4
NGC 513	80.3	12 μ m, RSA, BAT	9.09×10^{-14} ; 6	1.5×10^{-13} ; 2	0.53; 3	
IRAS01475–0740	23.3	12 μ m	6.49×10^{-14} ; 1	5.5×10^{-14} ; 2	0.83; 5	
NGC 788	55.0	RSA, BAT	1.80×10^{-13} ; 6	1.5×10^{-13} ; 17	0.71; 3	-1.43; 4
NGC 1068	12.3	RSA	1.90×10^{-11} ; 8 ^d	2.0×10^{-11} ; 2	0.88; 9	-1.89; 4
NGC 1125	46.2	12 μ m	4.04×10^{-13} ; 6	2.3×10^{-14} ; 7	0.50; 5	
ESO 417–G006	68.8	BAT	4.04×10^{-14} ; 10	2.3×10^{-14} ; 11	0.91; 5	
Mrk 1066	49.4	RSA	4.02×10^{-13} ; 10	2.4×10^{-13} ; 2	0.57; 9	-1.65; 12
NGC 1320	37.7	12 μ m, RSA	3.23×10^{-13} ; 1	1.2×10^{-13} ; 2	0.32; 5	-1.53; 4
NGC 1358	56.8	RSA	7.61×10^{-14} ; 8	2.0×10^{-13} ; 8	0.72; 3	-1.20; 4
NGC 1386	16.2	12 μ m, RSA	8.70×10^{-13} ; 8	2.7×10^{-13} ; 8	0.40; 3	-1.42; 4
NGC 1433	11.6	RSA	6.07×10^{-14} ; 8	2.1×10^{-14} ; 8	0.91; 5	
F04385–0828	63.8	12 μ m	8.56×10^{-14} ; 1	8.0×10^{-15} ; 2	0.50; 9	
NGC 1667	64.1	12 μ m, RSA	9.28×10^{-14} ; 8	9.1×10^{-15} ; 8	0.63; 3	
ESO 033–G02	76.5	12 μ m, BAT	1.44×10^{-13} ; 6	8.1×10^{-14} ; 2	1.0; 5	
NGC 2110	32.8	RSA, BAT	4.57×10^{-13} ; 10	1.7×10^{-13} ; 2	0.79; 3	-1.37; 4
Mrk 3	57.0	BAT	2.14×10^{-12} ; 10	3.5×10^{-12} ; 13	0.72; 3	-1.85; 4
NGC 2273	30.0	RSA	1.47×10^{-14} ; 8	2.8×10^{-13} ; 8	0.63; 3	
MGC+01–24–012	142.8	BAT	1.01×10^{-13} ; 10	9.2×10^{-14} ; 2	0.62; 3	
NGC 3081	32.5	RSA, BAT	9.89×10^{-13} ; 8	1.3×10^{-12} ; 17	0.60; 3	-1.82; 4
NGC 3079	19.4	RSA, BAT	1.53×10^{-13} ; 8	1.6×10^{-15} ; 8	0.18; 5	
IC 2560	35.1	RSA	5.43×10^{-13} ; 8	1.3×10^{-13} ; 8	0.63; 5	
NGC 3185	22.0	RSA	4.70×10^{-14} ; 8	5.0×10^{-14} ; 8	0.42; 5	
NGC 3393	51.4	RSA	1.87×10^{-12} ; 10	9.9×10^{-13} ; 2	0.87; 9	-2.00; 4
NGC 3486	10.6	RSA	3.30×10^{-14} ; 8	1.3×10^{-14} ; 8	0.72; 3	
NGC 3735	41.1	RSA	4.84×10^{-13} ; 8	3.7×10^{-14} ; 8	0.19; 5	
NGC 3941	15.6	RSA	9.35×10^{-15} ; 8	7.7×10^{-15} ; 8	0.66; 5	
NGC 4388	18.1	12 μ m, RSA, BAT	2.59×10^{-12} ; 8	5.9×10^{-13} ; 2	0.28; 9	-1.61; 4
NGC 4477	16.8	RSA	1.69×10^{-14} ; 8	1.9×10^{-14} ; 8	0.92; 5	
NGC 4501	20.7	12 μ m, RSA	3.98×10^{-14} ; 8	3.7×10^{-14} ; 8	0.54; 5	
NGC 4507	48.5	RSA, BAT	3.31×10^{-13} ; 8	8.9×10^{-13} ; 2	0.80; 3	-1.55; 4
Tol 1238–364	44.9	12 μ m, RSA	1.1×10^{-13} ; 6	4.1×10^{-13} ; 14	0.89; 3	
NGC 4698	41.7	RSA	2.04×10^{-14} ; 8	1.9×10^{-14} ; 8	0.63; 5	
NGC 4941	13.8	12 μ m, RSA	1.50×10^{-13} ; 8	1.4×10^{-13} ; 8	0.48; 3	
NGC 4939	41.0	RSA	4.30×10^{-13} ; 8	1.6×10^{-13} ; 8	0.51; 5	
NGC 4968	25.1	12 μ m	3.37×10^{-13} ; 6	1.9×10^{-13} ; 15	0.47; 5	
NGC 5135	56.3	12 μ m, RSA	5.83×10^{-13} ; 8	2.3×10^{-13} ; 2	0.80; 3	-1.78; 4
NGC 5347	36.7	12 μ m, RSA	6.7×10^{-14} ; 1	4.5×10^{-14} ; 2	0.74; 3	
NGC 5631	30.3	RSA	1.46×10^{-14} ; 8	4.5×10^{-15} ; 8	0.87; 5	
NGC 5643	16.9	RSA	8.16×10^{-13} ; 8	2.4×10^{-13} ; 8	0.95; 3	-1.71; 4
NGC 5728	36.2	RSA, BAT	1.29×10^{-12} ; 8	7.1×10^{-13} ; 2	0.53; 3	-1.54; 4
NGC 5899	39.8	RSA	2.63×10^{-13} ; 8	6.9×10^{-14} ; 8	0.38; 5	
NGC 6300	12.7	RSA	2.98×10^{-13} ; 8	2.2×10^{-13} ; 2	0.62; 3	-1.42; 4
IC 5063	46.6	12 μ m, RSA, BAT	1.17×10^{-12} ; 1	1.0×10^{-13} ; 2	0.71; 3	-1.70; 16

Table 1—Continued

name	Distance(Mpc) ^b	original sample(s)	F[O IV] ^c	F[OIII] ^c	b/a	logR _{O3}
Mrk 897	111.3	12 μ m	6.20×10^{-15} ; 6	5.9×10^{-15} ; 7	1.0; 5	
IRASF22017+0319	258.2	12 μ m	2.90×10^{-13} ; 6	2.3×10^{-13} ; 2	0.43; 5	
MGC–03–58–7	132.9	12 μ m, RSA	1.20×10^{-13} ; 1	4.8×10^{-13} ; 2	0.80; 5	
NGC 7582	18.8	12 μ m, RSA, BAT	2.22×10^{-12} ; 8	1.3×10^{-13} ; 2	0.46; 3	–1.76; 4
NGC 7590	25.3	12 μ m, RSA	6.88×10^{-14} ; 8	1.1×10^{-14} ; 8	0.35; 5	
NGC 7682	72.3	BAT	1.62×10^{-13} ; 10	2.3×10^{-13} ; 2	0.85; 3	–1.75; 4
NGC 7743	21.4	RSA	3.30×10^{-14} ; 8	7.9×10^{-15} ; 8	0.87; 5	

^aSecond number in column is the reference for the value, as follows: 1. Tommasin et al. (2010); 2. Bonatto & Pastoriza (1997); 3. Kirhakos & Steiner (1990); 4. Nagao et al. (2001), and references therein; 5. NED; ; 6. Tommasin et al. (2008); 7. Gu et al. (2006); 8. Diamond-Stanic et al. (2009); and references therein; 9. de Zotti & Gaskell (1985); 10. Meléndez et al. (in prep.); 11. Stauffer (1982); 12. Goodrich & Osterbrock (1983); 13. Vaceli et al. (1997); 13. Ho et al. (1997); 14. Cid Fernandes et al. (2001); 16. Phillips, Charles & Baldwin (1983); Whittle (1992).

^bDistances are mean values from literature (see NED) or, if none are available, calculated from redshift, assuming $H_0 = 71 \text{ km s}^{-1} \text{ Mpc}^{-1}$.

^cFlux in units of $\text{ergs cm}^{-2} \text{ s}^{-1}$.

Table 2. Properties of the Seyfert 1 Galaxies in the Sample

name	Distance(Mpc) ^b	original sample(s)	F[O IV] ^c	F[OIII] ^c	b/a	logR _{O3}
Mrk 335	109.0	12 μ m, BAT	7.28×10^{-13} ; 1	2.3×10^{-13} ; 17	0.86; 3	-1.16; 4
Mrk 352	63.0	BAT	2.60×10^{-15} ; 10	4.9×10^{-14} ; 17	0.73; 3	
F9	177.0	BAT	6.08×10^{-14} ; 10	2.4×10^{-13} ; 17	0.80; 3	-0.92; 4
Mrk 590	112.0	BAT	1.79×10^{-14} ; 10	5.4×10^{-14} ; 2	0.82; 3	-0.70; 4
ESO 545–G-13	101.8	12 μ m	1.15×10^{-13} ; 6	2.6×10^{-13} ; 2	0.82; 5	
NGC 931	51.5	12 μ m, BAT	4.30×10^{-13} ; 6	1.8×10^{-13} ; 2	0.27; 3	
IC 1816	71.4	BAT	1.65×10^{-13} ; 10	5.7×10^{-13} ; 2	0.86; 5	
NGC 1566	11.8	RSA	8.88×10^{-14} ; 8	1.7×10^{-13} ; 8	0.79; 9	-0.80; 4
3C 120	139.5	12 μ m, BAT	1.14×10^{-12} ; 1	3.2×10^{-13} ; 2	0.75; 5	-1.06; 4
Mrk 6	79.5	12 μ m, BAT	5.00×10^{-13} ; 6	7.9×10^{-13} ; 2	0.50; 3	-1.75; 4
Mrk 79	93.8	12 μ m, BAT	5.10×10^{-13} ; 1	5.8×10^{-13} ; 2	0.61; 3	-1.34; 4
IC 486	106.0	BAT	1.12×10^{-13} ; 10	2.0×10^{-13} ; 2	0.66; 5	
NGC 3227	20.9	RSA, BAT	5.71×10^{-13} ; 8	9.4×10^{-13} ; 8	0.40; 3	-1.50; 4
NGC 3516	38.9	12 μ m, RSA, BAT	5.60×10^{-13} ; 8	3.5×10^{-13} ; 8	0.71; 3	-1.42; 4
NGC 3783	38.5	RSA, BAT	2.80×10^{-13} ; 8	8.3×10^{-13} ; 8	0.89; 3	-1.30; 4
NGC 4051	17.0	12 μ m, RSA, BAT	2.64×10^{-13} ; 8	4.4×10^{-13} ; 8	0.68; 9	
NGC 4151	12.1	RSA, BAT	2.08×10^{-12} ; 8	1.1×10^{-11} ; 8	0.74; 9	-1.66; 4
NGC 4235	35.1	RSA, BAT	4.33×10^{-14} ; 8	2.0×10^{-14} ; 8	0.25; 9	-0.55; 4
Mrk 766	54.5	12 μ m, RSA, BAT	4.65×10^{-13} ; 1	4.5×10^{-13} ; 2	0.85; 9	-1.53; 4
NGC 4593	44.0	12 μ m, RSA, BAT	1.32×10^{-13} ; 8	1.3×10^{-13} ; 8	0.78; 9	
MCG–6–30–15	32.7	12 μ m, BAT	2.00×10^{-13} ; 1	7.5×10^{-14} ; 2	0.60; 9	-1.11; 4
IC 4329A	68.0	12 μ m, BAT	1.05×10^{-12} ; 1	3.5×10^{-13} ; 2	0.20; 3	
NGC 5548	70.6	12 μ m, RSA, BAT	1.50×10^{-13} ; 1	7.3×10^{-13} ; 2	0.83; 9	-0.99; 4
Mrk 817	132.9	12 μ m, BAT	6.00×10^{-14} ; 6	1.3×10^{-13} ; 2	0.89; 3	-1.37; 4
Mrk 841	154.0	BAT	2.29×10^{-13} ; 10	3.4×10^{-13} ; 2	0.94; 3	-1.04; 4
ESO 140–G043	47.8	BAT	2.75×10^{-13} ; 10	2.8×10^{-13} ; 17	0.50; 3	-1.40; 4
NGC 6814	68.9	RSA	2.13×10^{-13} ; 8	7.0×10^{-14} ; 8	0.86; 3	-1.15; 4
NGC 6860	61.3	12 μ m, BAT	1.17×10^{-13} ; 1	3.5×10^{-13} ; 2	0.62; 5	-1.17; 4
Mrk 509	141.3	12 μ m, RSA, BAT	2.85×10^{-13} ; 8	8.6×10^{-13} ; 8	0.85; 9	
NGC 7469	67.1	RSA, BAT	3.67×10^{-13} ; 8	5.9×10^{-13} ; 8	0.58; 3	-1.47; 4

^aReferences: same as in Table 1.

^bDistances are mean values from literature (see NED) or, if none are available, calculated from redshift, assuming $H_0 = 71 \text{ km s}^{-1} \text{ Mpc}^{-1}$.

^cFlux in units of $\text{ergs cm}^{-2} \text{ s}^{-1}$.

^dFlux from Infrared Space Observatory/Short Wave Spectrometer data (Lutz et al. 2000).

Table 3. Properties of the Seyfert 1.8 and 1.9 Galaxies in the Sample^a

name	Distance(Mpc) ^b	original sample(s)	F[O IV] ^c	F[OIII] ^c	b/a	logR _{O3}
NGC 1194	57.4	12 μ m, BAT	1.51×10^{-13} ; 1	1.5×10^{-14} ; 2	0.48; 5	
NGC 1365	17.7	12 μ m, RSA, BAT	1.58×10^{-12} ; 8	6.2×10^{-14} ; 8	0.56; 3	
NGC 2639	47.0	12 μ m, RSA	3.27×10^{-14} ; 8	1.9×10^{-14} ; 8	0.50; 3	
NGC 2992	30.5	RSA	1.08×10^{-12} ; 8	9.5×10^{-13} ; 2	0.31; 5	-1.65; 4
NGC 3660	51.9	12 μ m	3.61×10^{-14} ; 6	3.5×10^{-14} ; 2	0.83; 3	
NGC 3982	21.8	12 μ m, RSA	2.00×10^{-14} ; 1	2.0×10^{-13} ; 2	0.82; 3	-2.80; 4
NGC 4138	15.6	RSA, BAT	4.27×10^{-14} ; 8	1.6×10^{-14} ; 8	0.65; 5	
NGC 4168	28.0	RSA	1.39×10^{-14} ; 8	2.4×10^{-15} ; 8	0.78; 5	
NGC 4395	4.2	RSA, BAT	4.23×10^{-14} ; 8	1.4×10^{-13} ; 8	0.83; 5	
NGC 4565	13.2	RSA	2.09×10^{-14} ; 8	1.5×10^{-14} ; 8	0.12; 5	
NGC 4639	22.3	RSA	1.54×10^{-14} ; 8	7.5×10^{-15} ; 8	0.68; 5	
NGC 5033	20.6	RSA	1.59×10^{-13} ; 8	5.3×10^{-14} ; 8	0.47; 3	
MCG-03-34-64	70.0	12 μ m	1.15×10^{-12} ; 1	1.6×10^{-12} ; 2	0.80; 5	
NGC 5273	17.7	RSA	3.72×10^{-14} ; 8	1.2×10^{-13} ; 8	0.82; 9	
NGC 6890	31.8	12 μ m, RSA	1.00×10^{-13} ; 8	1.9×10^{-13} ; 8	0.75; 3	
NGC 7314	19.0	12 μ m, RSA, BAT	4.91×10^{-13} ; 8	6.5×10^{-14} ; 2	0.43; 3	-2.67; 4

^aReferences: same as in Tables 1 and 2

^bDistances are mean values from literature (see NED) or, if none are available, calculated from redshift, assuming $H_0 = 71 \text{ km s}^{-1} \text{ Mpc}^{-1}$.

^cFlux in units of $\text{ergs cm}^{-2} \text{ s}^{-1}$.

Table 4. Properties of the LINERS in the Sample^a

name	Distance(Mpc) ^b	original sample(s)	F[O IV] ^c	F[OIII] ^c	b/a
NGC 2655	24.4	RSA	6.25×10^{-14} ; 8	3.9×10^{-14} ; 8	0.84; 5
NGC 3031	3.7	RSA	4.99×10^{-14} ; 8	2.2×10^{-13} ; 8	0.52; 5
NGC 4258	7.9	RSA	7.99×10^{-14} ; 8	1.0×10^{-13} ; 8	0.39; 5
NGC 4579	16.8	RSA	2.83×10^{-14} ; 8	7.8×10^{-14} ; 8	0.80; 5
NGC 5005	17.5	12 μ m, RSA	1.99×10^{-14} ; 8	4.7×10^{-14} ; 8	0.48; 5
NGC 6951	14.1	RSA	8.37×10^{-14} ; 8	7.0×10^{-15} ; 8	0.82; 5
NGC 7213	22.0	12 μ m, RSA, BAT	2.11×10^{-14} ; 8	3.4×10^{-13} ; 8	0.92; 3
NGC 7410	20.1	RSA	4.63×10^{-14} ; 8	1.9×10^{-14} ; 8	0.31; 5

^aReferences: same as in Tables 1 and 2.

^bDistances are mean values from literature (see NED) or, if none are available, calculated from redshift, assuming $H_0 = 71 \text{ km s}^{-1} \text{ Mpc}^{-1}$.

^cFlux in units of $\text{ergs cm}^{-2} \text{ s}^{-1}$.

Table 5. Estimated Hydrogen Column Densities

name	$\log N_H$ (dust ^a)	$\log N_H$ (X-ray ^a)
Mrk 348	20.88	
IRAS 00521–7054	21.11	
NGC 424	– ^b	21.10
NGC 513	20.49	
IRAS01475–0740	21.15	
NGC 788	21.15	
NGC 1068	21.00	21.30
NGC 1125	21.75	
ESO417–G006	21.30	
Mrk 1066	21.30	
NGC 1365	21.81	21.60
NGC 1433	21.45	
F04385–0828	21.70	
NGC 1667	21.69	
ESO033–G02	21.32	
NGC 2110	21.43	
Mrk 3	20.53	21.45
NGC 2273	19.92	
MCG01–24–012	21.11	
NGC 2992	21.11	21.54
NGC 3081	20.88	
IC 2560	21.53	21.45
NGC 3393	21.34	
NGC 3486	21.43	
NGC 3941	21.15	
NGC 4477	20.97	
NGC 4501	21.08	
NGC 4507		20.11
NGC 4698	21.08	
NGC 4939	21.43	
MCG–03–34–64	20.81	21.45
NGC 5135	21.43	
NGC 5347	21.26	
NGC 5631	21.48	
NGC 5643	21.49	
NGC 5728	21.32	
NGC 6300	21.23	
IC 5063	21.70	
Mrk 897	21.11	
NGC 7582	21.76	21.70
NGC 7682	20.74	20.20
NGC 7743	21.53	

^aIn units of cm^{-2} . For details, see text.

^b[O III]/[O IV] ratio > mean for Seyfert 1s.

Table 6. O VII λ 22.1 Å fluxes^a

name	Flux	Reference
ESO 362–G018	$6.52^{+5.23}_{-3.34}$	1
IC 2560	$1.70^{+1.51}_{-0.97}$	1
MCG–03–34–64	$3.48^{+3.35}_{-1.37}$	1
Mrk 3	$6.62^{+2.39}_{-1.68}$	1
NGC 1068	$108.^{+6.36}_{-6.11}$	1
NGC 1365	$2.16^{+0.44}_{-0.41}$	1
NGC 2992	$2.01^{+2.34}_{-1.50}$	1
NGC 3227	$1.96^{+1.22}_{-0.96}$	1
NGC 3516	$3.78^{+4.31}_{-3.25}$	2
NGC 3783	$9.21^{+2.49}_{-2.49}$	3
NGC 4051	$11.3^{+3.32}_{-2.86}$	4
NGC 4151	$45.5^{+2.30}_{-2.20}$	5
NGC 424	$2.83^{+3.92}_{-1.74}$	1
NGC 4507	$8.57^{+3.26}_{-2.58}$	1
NGC 5548	$7.91^{+1.08}_{-1.08}$	6
NGC 7582	$1.36^{+0.61}_{-0.52}$	1
NGC 7682	$4.05^{+4.48}_{-3.20}$	1

^aIn units of 10^{-14} ergs cm⁻² s⁻¹

^b1. This paper; 2. Turner et al. (2003); 3. Kaspi et al. (2002); Lobban et al. (in prep.); 5. Armentrout et al. (2007); 6. Steenbrugge et al. (2005).

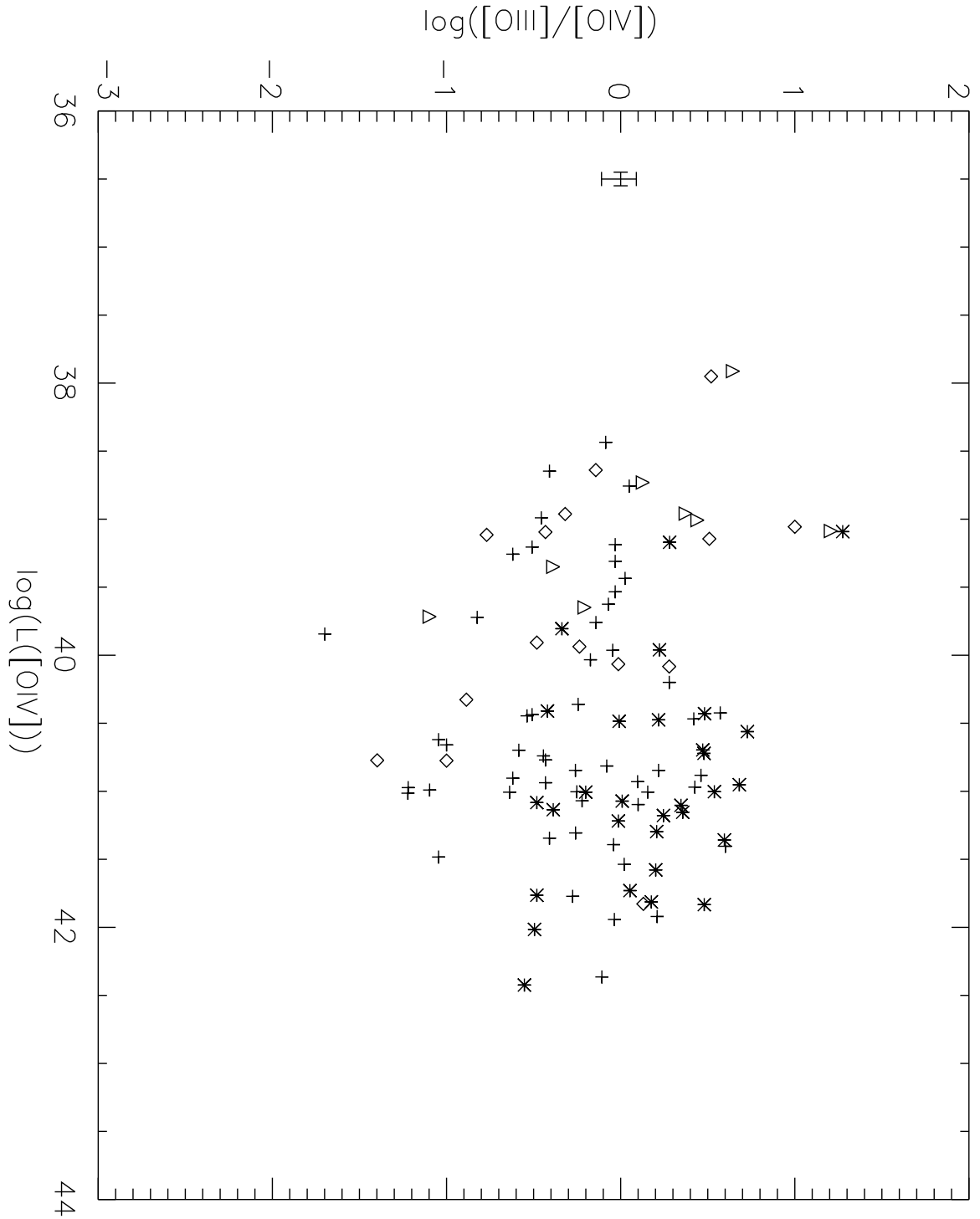


Fig. 1

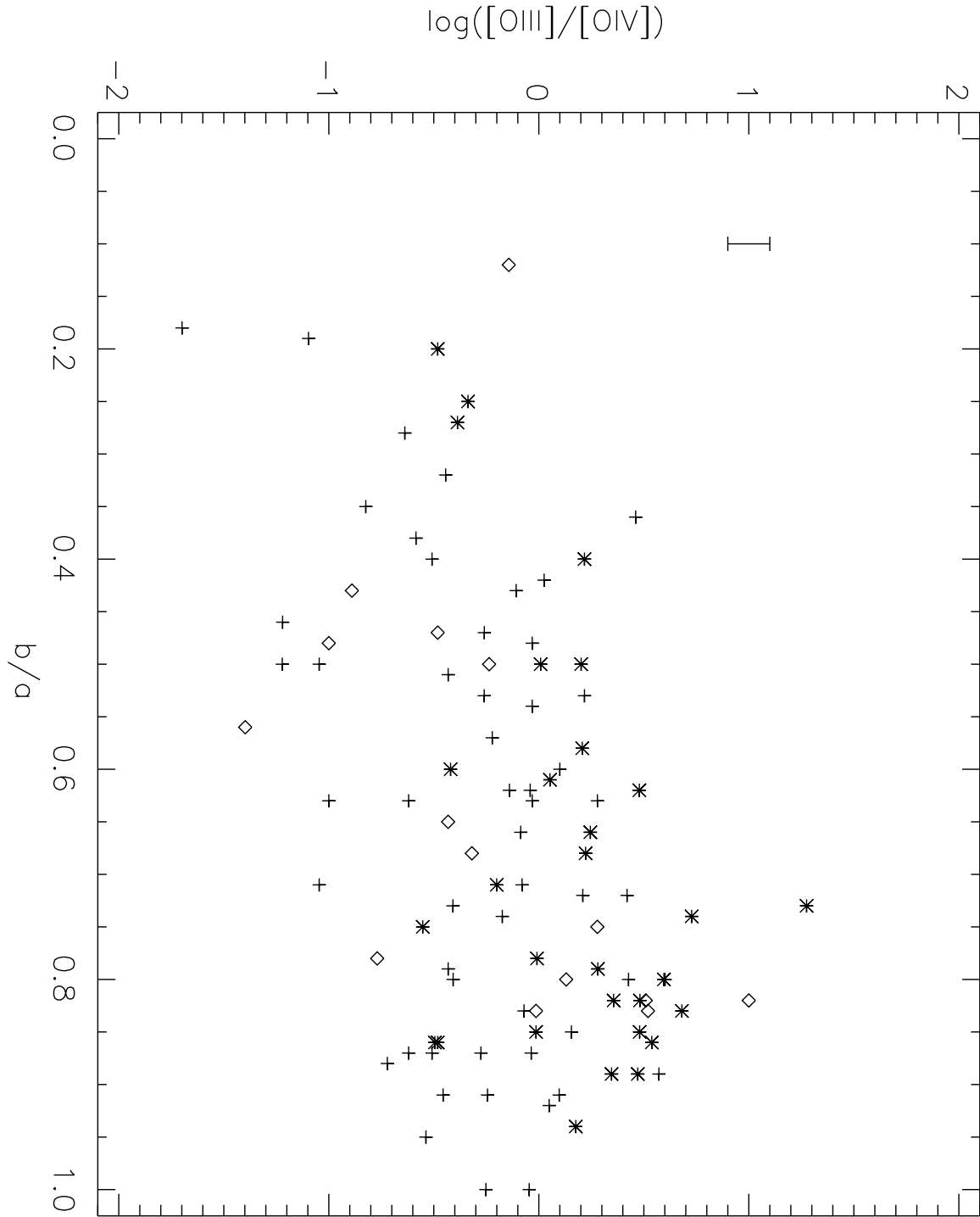


Fig. 2

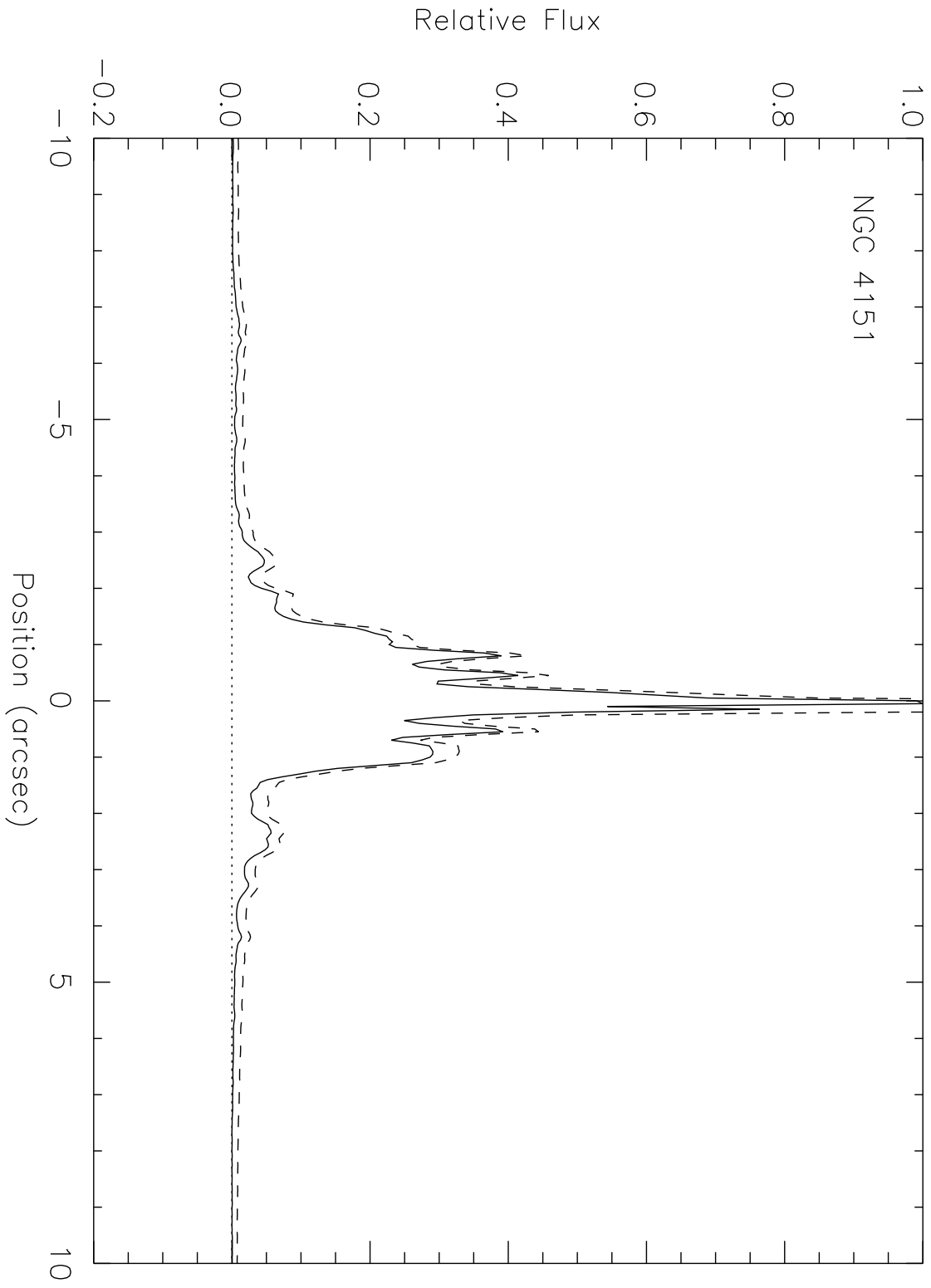


Fig. 3

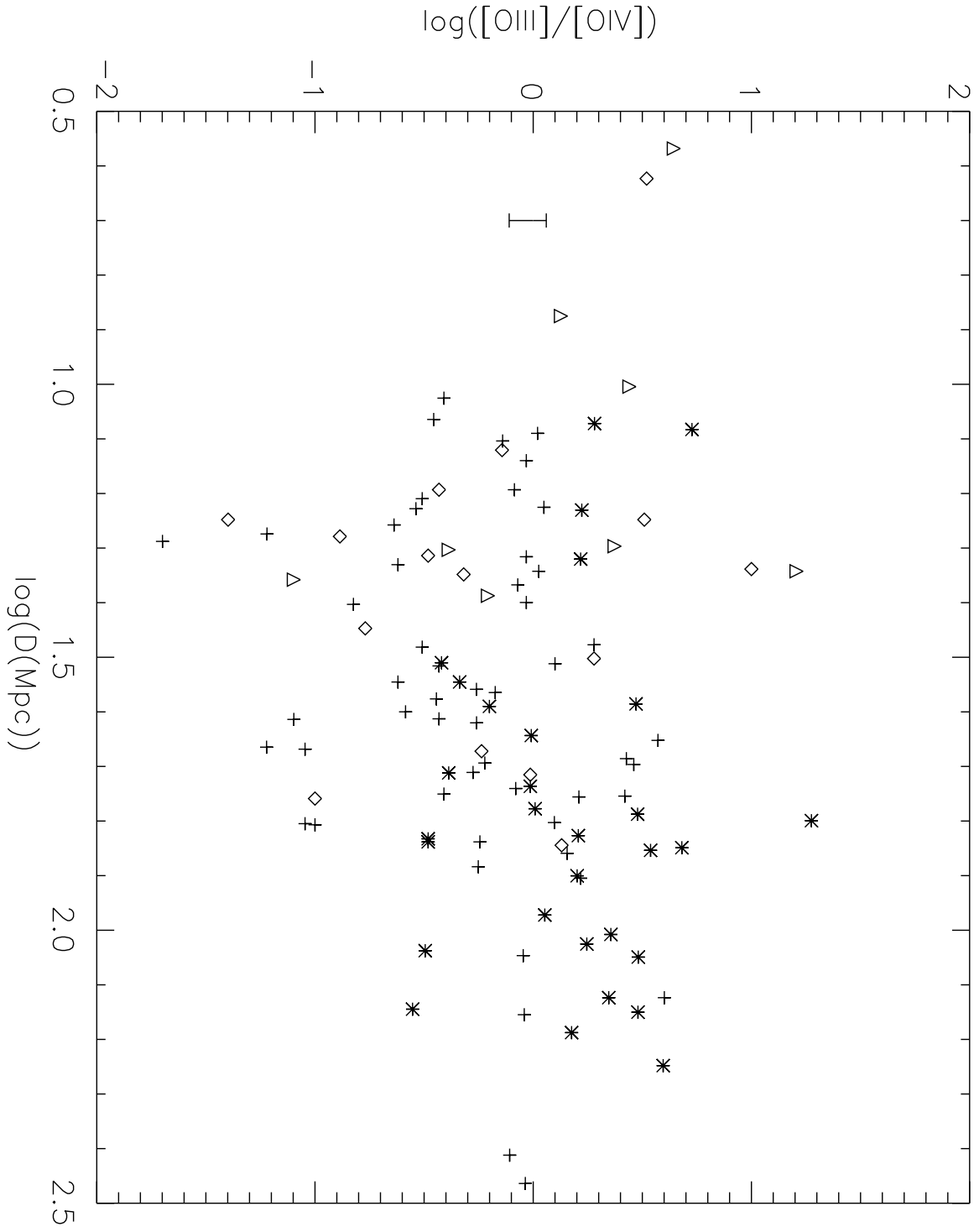


Fig. 4

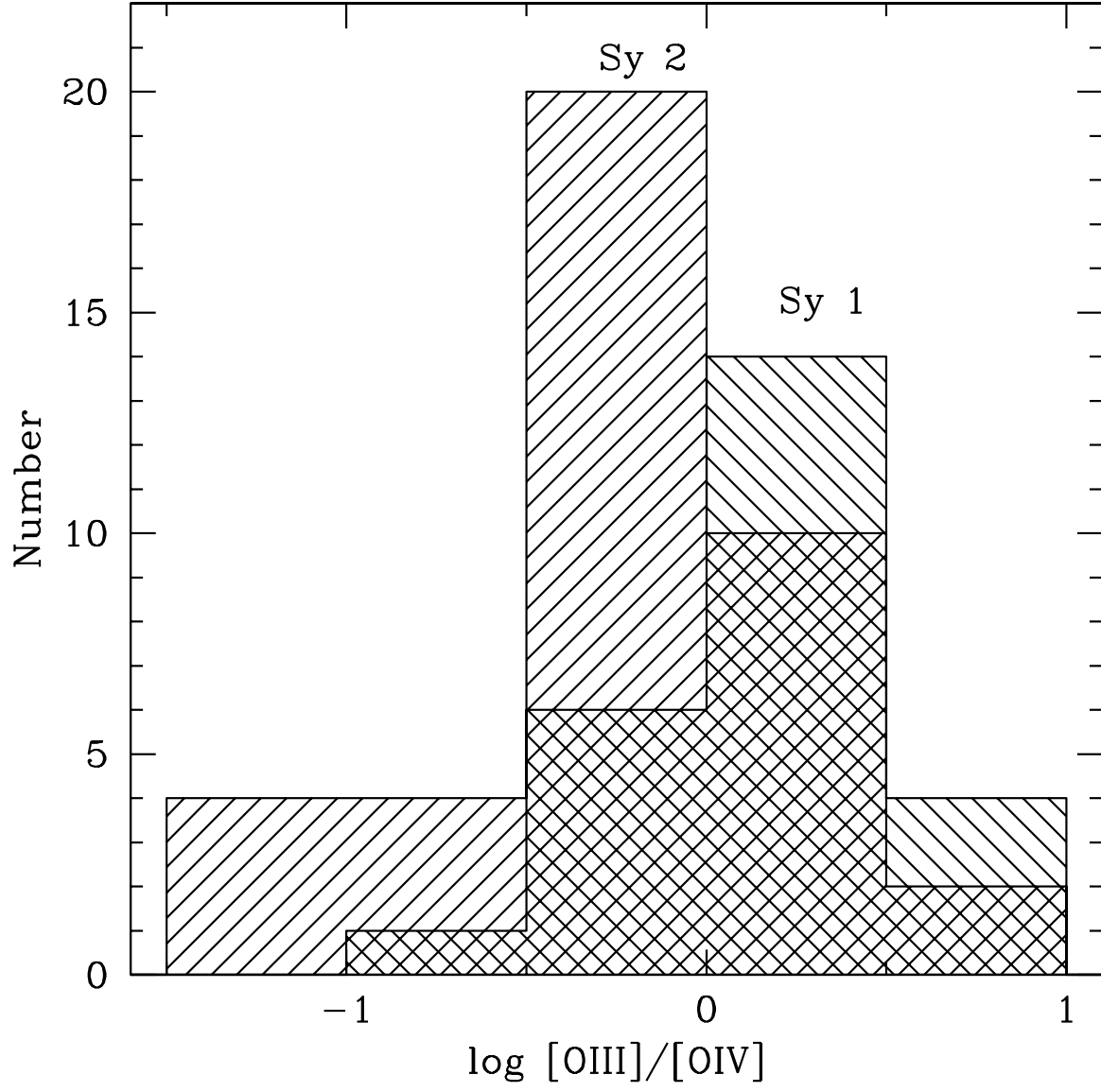


Fig. 5

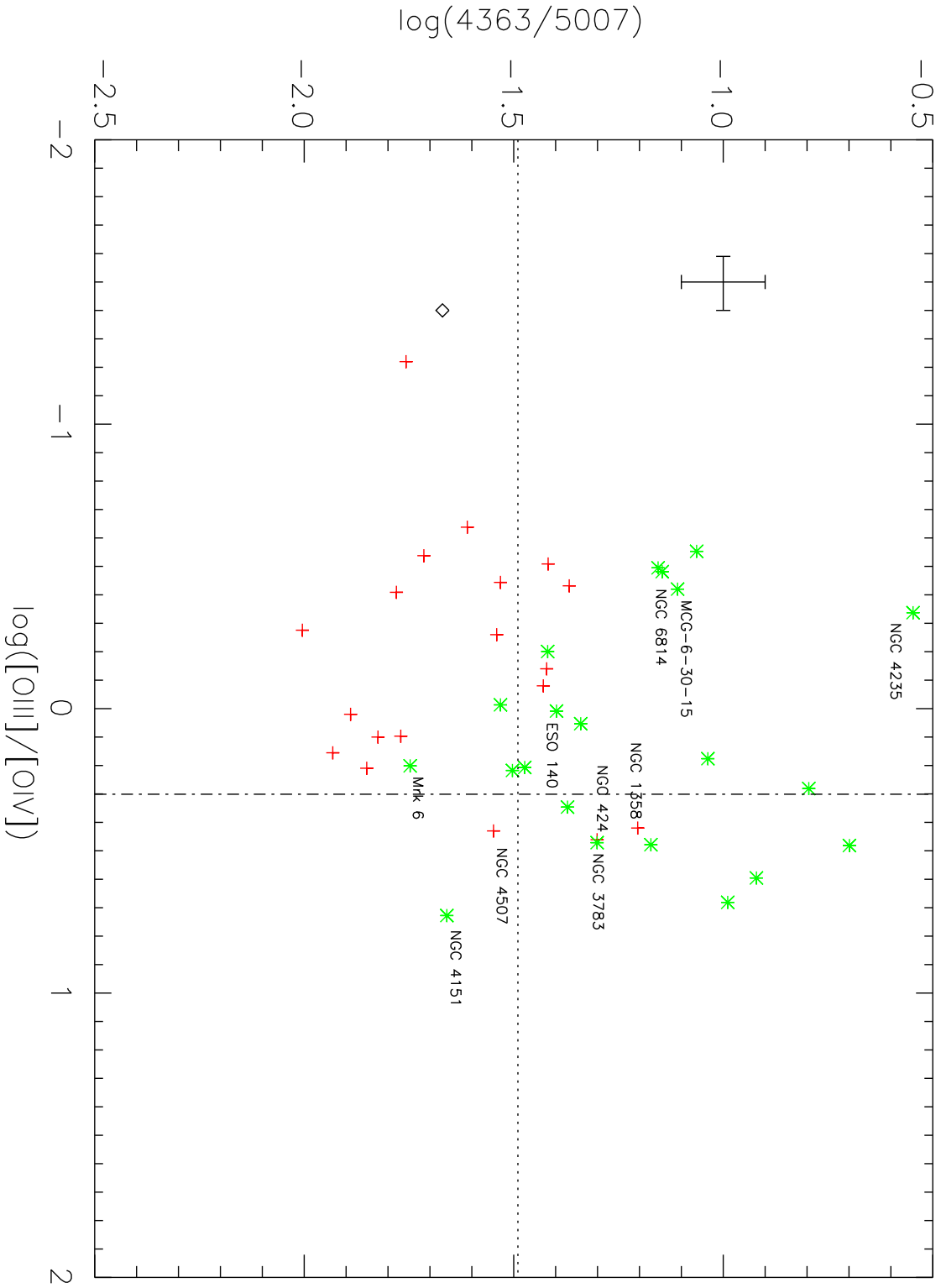


Fig. 6

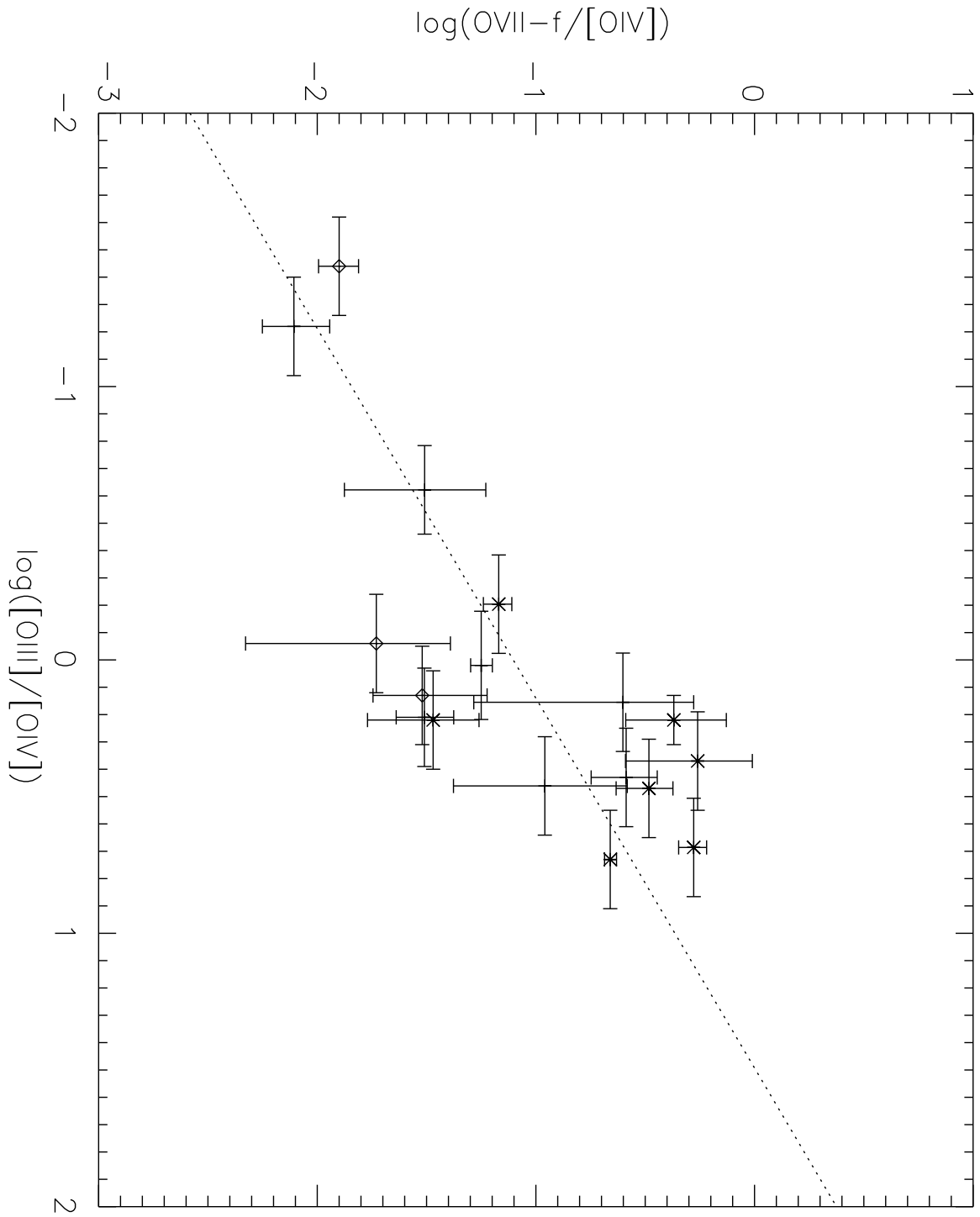


Fig. 7